PERGAMON

International Journal of Multiphase Flow 26 (2000) 2005–2047

International Journal of Multiphase Flow

www.elsevier.com/locate/ijmulflow

Potential flow around a deforming bubble in a Venturi

J.D. Sherwood

Schlumberger Cambridge Research, High Cross, Madingley Road, Cambridge, CB3 OEL, UK

Received 10 February 1999; received in revised form 9 December 1999

Abstract

The differential pressure between the entrance and throat of a Venturi will fluctuate if the liquid flowing through the Venturi contains bubbles. This paper reports computations of the pressure fluctuation due to the passage of a single bubble. The liquid is assumed inviscid and its velocity, assumed irrotational, is computed by means of a boundary integral technique. The liquid velocity at the entrance to the Venturi is assumed constant and uniform across the pipe, as is the pressure at the outlet. The bubble is initially far upstream of the Venturi and moves with velocity equal to that of the liquid. Buoyancy is neglected. If the bubble is sufficiently small that interactions with the Venturi walls may be neglected, a simple one-dimensional model for the bubble velocity is in good agreement with the full boundary integral computations. The differential pressure (taken to be positive) decreases when the bubble enters the converging section of the Venturi, and then increases to a value higher than for liquid alone as the bubble passes the pressure measurement position within the throat. The changes can be estimated using the one-dimensional model, if the bubble is small. The bubble is initially spherical (due to surface tension) but is perturbed by the low pressure within the Venturi throat. In the absence of viscosity, the bubble oscillates after leaving the Venturi. The quadrupole oscillations of the bubble are similar in frequency to those of a bubble in unbounded fluid; the frequency of the monopole oscillations is modified by the presence of the pipe walls. Numerical results for the frequency of monopole oscillations of a bubble in a uniform tube of finite length are in good agreement with analytic predictions, as is the computed drift of the oscillating bubble.

Keywords: Bubble; Venturi; Potential law

E-mail address: sherwood@cambridge.scr.slb.com (J.D. Sherwood).

0301-9322/00/$ - see front matter
PII: S0301-9322(99)00123-8

1. Introduction

The use of a Venturi for flow measurement at high Reynolds numbers is standard practice in single phase flow. Multiphase flows are harder to measure, since the mean density of the flowing mixture depends upon the volume fraction of the various phases, which are likely to be moving relative to one another. Nevertheless the measured differential pressure between the entrance and throat of a Venturi can lead to flow rate estimates when combined with information from other sources. Recent practical devices are reviewed by Thorn et al. (1997) and some theoretical background is provided by Boyer and Lemonnier (1996).

The differential pressure within a Venturi will fluctuate due to the passage of bubbles: the main aim of this paper is to study the fluctuation caused by the passage of a single deformable gas bubble when the bubble and the surrounding inviscid, incompressible liquid flow through a Venturi. The bubble is assumed to move along the axis of the Venturi so that the problem is axisymmetric, and the liquid velocity is assumed irrotational. The bubble motion and the potential velocity field in the surrounding liquid will be computed by means of a boundary integral technique. Results so obtained will be compared with those predicted by a simpler, one-dimensional model that neglects interactions between the bubble and the walls of the Venturi. This will prepare the way for simpler computations of the motion of undeformable bubbles away from the axis of the Venturi (Soubiran and Sherwood, 2000).

Buoyancy forces will be neglected, since in the absence of viscous drag a bubble would have no steady rate of rise. Although drag could be estimated from the viscous dissipation in the potential flow field around the bubble (Batchelor, 1973, p. 368), such a calculation would neglect the contribution to dissipation from the boundary layers at the rigid walls of the pipe. The bubble is assumed to contain an ideal, isothermal gas. Realistic flow rates are sufficiently high (see Section 3), that it might be more appropriate to assume adiabatic deformation for all but the smallest bubbles. A few simulations of bubbles under adiabatic conditions were performed, but are not presented here: results were qualitatively the same as for an isothermal gas. The pressure within the gas is always greater than zero. However, negative pressures might occur in the liquid if the ambient pressure is sufficiently small: the possibility of cavitation was ignored.

In the petroleum industry, the flow to be measured might consist of oil together with gas that has come out of solution as the oil flows up a well towards the surface. Further gas might come out of solution as the mixture enters the low pressure region in the Venturi throat. This was neglected. The change in pressure within a Venturi is typically small compared to the hydrostatic pressure change corresponding to the vertical height of a 1 km well.

Realistic multiphase flows may well contain a high volume fraction of gas, rather than solitary bubbles, and flow rates may be high. Such flows are usually far from steady, and turbulent churn flow is likely. The results obtained here are therefore somewhat removed from realistic flows.

We start in Section 2 by considering two simple one-dimensional models which will help our understanding of the full potential flow computations. Order of magnitude estimates for typical flow rates are given in Section 3. Details of the boundary integral scheme are discussed in Section 4 and numerical results presented in Section 5. In Appendix A, an analysis of the

resonant frequency of oscillation of a small bubble in a pipe is used to check the accuracy of the full potential flow computations.

2. Simple one-dimensional models

2.1. A bubble in a Venturi

Kuo and Wallis (1988) studied the motion of individual bubbles through a nozzle, and compared experimental results against the predictions of a one-dimensional model which included steady and unsteady viscous drag, added mass (acceleration reaction), buoyancy and pressure forces acting on the bubble. A similar analysis was presented by Kowe et al. (1988) for the case of steady viscous drag. We shall ignore buoyancy and viscous forces, and consider a simplified version of the model in which a bubble moves under the action of the pressure and added mass.

Figs. 1 and 2 show a Venturi with inlet diameter $2\tilde{a}$: we non-dimensionalise all lengths by $\tilde{a}$. The pipe has a radius

$$R_{\mathrm{p}} = \begin{cases} 1 & 0 < x < x_1 \\ 1 - \frac{(x-x_1)(1-\beta)}{x_2-x_1} & x_1 < x < x_2 \\ \beta & x_2 < x < x_3 \\ 1 - \frac{(x_4-x)(1-\beta)}{x_4-x_3} & x_3 < x < x_4 \\ 1 & x_4 < x < x_5 \end{cases}, \tag{1}$$

where β is the non-dimensional radius of the Venturi throat, and x is distance along the axis. We assume that the liquid velocity is uniform across the cross-section, and equal to $\tilde{U}$ at the entrance. We non-dimensionalise all velocities by $\tilde{U}$, so that the dimensionless liquid velocity at the entrance is $u_{\mathrm{l}} = 1$. Time is non-dimensionalised by $\tilde{a}/\tilde{U}$, densities by $\tilde{\rho}_{\mathrm{l}}$ and pressures by $\tilde{\rho}_{\mathrm{l}}\tilde{U}^2$.

We consider an incompressible, spherical gas bubble of radius R_0 and density ρ_{g} moving along the axis of the pipe. The forces acting on a bubble (in unbounded liquid) are discussed by Batchelor (1973, p. 409) and Auton et al. (1988). The lift force is zero in irrotational flow, and we neglect drag. If the centre of the bubble is at $x_{\mathrm{b}}(t)$, the equation of motion for the

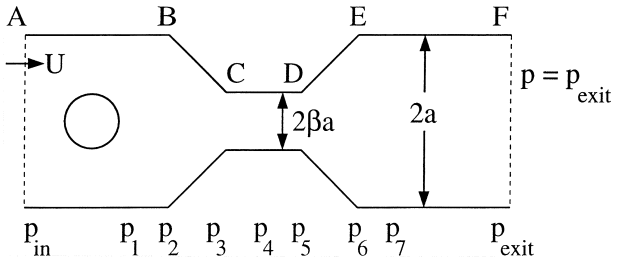

Fig. 1. The Venturi, shown with a bubble on the centreline, and with a series of pressure tappings $p_1, \ldots, p_7$ at which the wall pressure is computed.

bubble becomes

$$\tfrac{4}{3}\pi R_0^3 \rho_g \tfrac{d^2 x_b}{dt^2} = \tfrac{4}{3}\pi R_0^3 \rho_l \left[\frac{D_l u_l}{Dt} - C_m \left(\frac{d^2 x_b}{dt^2} - \frac{D_l u_l}{Dt} \right) \right], \tag{2}$$

where C_m is the added mass coefficient and $D_l u_l / Dt = \partial u_l / \partial t + u_l \partial u_l / \partial x$ evaluated at the instantaneous position $x_b(t)$ of the bubble. The left-hand side of Eq. (2) represents the mass–acceleration of the bubble. The first term on the right-hand side represents the force due to the pressure gradient within the liquid (in the absence of the bubble); the second term is the acceleration reaction (added mass force) due to acceleration of the bubble relative to the liquid. The liquid velocity is assumed steady and we now set the gas density $\rho_g = 0$. The governing equation becomes

$$\frac{d^2 x_b}{dt^2} = \left(\frac{1 + C_m}{C_m} \right) u_l \frac{\partial u_l}{\partial x} \tag{3}$$

with

$$x_b = 1, \qquad v_b \equiv \frac{dx_b}{dt} = 1 \quad \text{at} \quad t = 0$$

as initial conditions for a bubble starting at $x_b = 1$ with velocity v_b equal to the liquid velocity. If we assume that the bubble is small compared to the radius of the pipe, then $C_m = 1/2$ is constant, and integrating Eq. (3) leads to

$$v_b^2 \equiv \left(\frac{dx_b}{dt} \right)^2 = \left(\frac{1 + C_m}{C_m} \right) u_l^2(x_b) - \frac{1}{C_m}. \tag{4}$$

Note that the velocity of the bubble can be expressed in terms of the local liquid velocity $u_l(x_b)$: when C_m is constant the inertia of the bubble is a fixed fraction of the inertia of the liquid it has replaced. If we assume that flow is uniform across the cross-section of the pipe, then

$$u_l = R_p^{-2}. \tag{5}$$

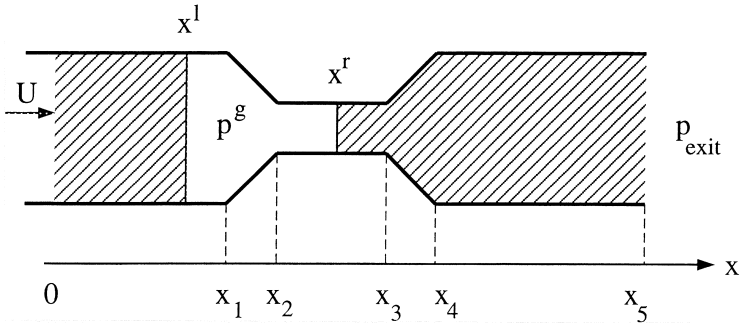

Fig. 2. Schematic of the one-dimensional slug model considered in Section 2.2.

Fig. 3 shows the predicted velocity of a bubble in a Venturi in which the converging section, throat and diverging section all have length 1, for various values of the non-dimensional throat radius β. We see that in the converging section the bubble accelerates faster than the liquid since the added mass of the bubble is only half the mass of the liquid it has replaced. Thus, when $\beta = 0.5$ the unperturbed liquid velocity in the throat is $u_l = 4.0$, whereas the bubble velocity is $v_b = 6.78$. Eq. (4) can be integrated numerically in order to find the bubble position $x_b(t)$ and results of this simple model will be compared against the potential flow computations in Section 5. Although one could extend the model to allow the bubble to expand in the low-pressure region of the throat, the radial growth of the bubble would be affected by the presence of the pipe walls, as discussed in Appendix A in the context of monopole oscillations of a bubble in a pipe. Such an extension will not be attempted here.

2.2. A one-dimensional slug model

The full numerical computations of Section 5 predict that, after passing through the Venturi, the bubble will oscillate with a frequency which increases as the bubble moves towards the exit of the Venturi. The reasons for this can be most easily demonstrated by means of a one-dimensional slug model. Fig. 2 shows a single slug of gas sandwiched between two liquid slugs passing through a Venturi. The velocity is assumed uniform across the cross-section of the pipe, so that all interfaces remain plane and interfacial tension can be ignored. The gas density $\rho_g = 0$ so that the velocity of sound is infinite within the gas, which is therefore at uniform pressure p^g. The liquid is incompressible with non-dimensional density $\rho_l = 1$. The velocity $U = 1$ at the entrance is constant, as is the pressure p_{exit} at the exit. These boundary conditions are intended to represent laboratory experiments in which fluid is supplied at constant flow rate by

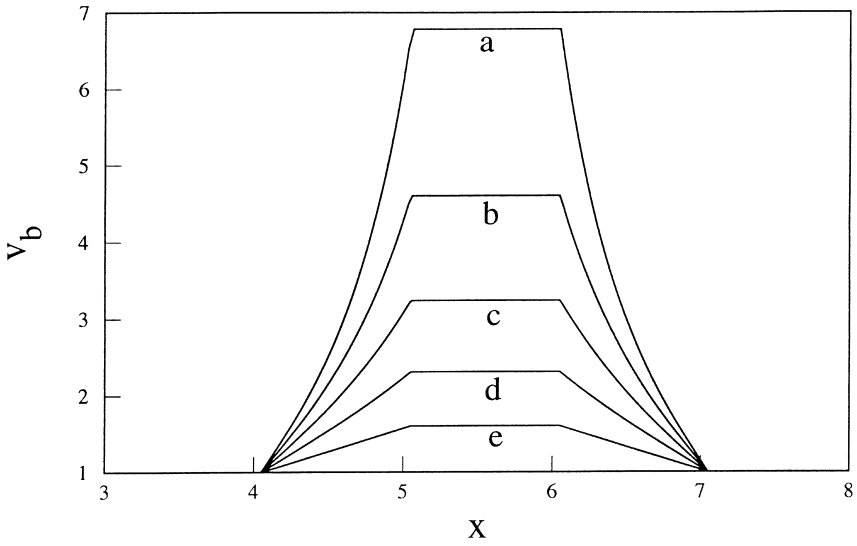

Fig. 3. The velocity v_b of a bubble, predicted by the one-dimensional model of Section 2.1, in a Venturi with dimensions $x_1 = 4.05$, and converging, throat and diverging sections all of length 1.0. Added mass coefficient $C_m = 0.5$. Curves correspond to (a) $\beta = 0.5$, (b) $\beta = 0.6$, (c) $\beta = 0.7$, (d) $\beta = 0.8$, (e) $\beta = 0.9$.

powerful pumps, and fluid exits from the Venturi at atmospheric pressure. Alternatively a choke might be fitted at the exit in order to raise the pressure within the apparatus. In this case any fluctuations in flow due to the presence of a bubble will lead to fluctuations in the pressure drop across the choke and (possibly) changes in the flow rates supplied by a pump. If the compliances of the choke and pump are known, such effects could be incorporated. However, here we shall keep to the simpler boundary conditions given above.

Initially the gas is far upstream of the Venturi and everything travels at velocity U (apart from the liquid within the Venturi). Similarly the pressure everywhere (apart from the Venturi) is p_{exit}. Once the gas enters the low pressure region within the Venturi, it expands and the system is perturbed. The system subsequently behaves as an oscillator, with inertia provided by the liquid between the gas and the exit and with the restoring force provided by the compressible gas.

The geometry of the Venturi is given as before by Eq. (1) and the non-dimensional cross-sectional area of the pipe is $A(x) = \pi R_{\text{p}}^2$. In the computations presented here we assume that the converging, throat and diverging sections of the Venturi all have length 1 and we take $\beta = 1/2$.

The gas slug occupies the region between x^{l} and x^{r} and has volume

$$V = \int_{x^{\text{l}}}^{x^{\text{r}}} A(x)\,\mathrm{d}x. \tag{6}$$

We assume isothermal deformation of the gas. The initial pressure, length and volume of the gas slug are p_{exit}, L and $V_0 = L\pi$, and at time t the pressure within the gas is

$$p^{\text{g}} = \frac{V_0 p_{\text{exit}}}{V} = \frac{L p_{\text{exit}}}{x^{\text{r}} - x^{\text{l}}}. \tag{7}$$

There are two slugs of liquid. The first occupies the region $x < x^{\text{l}}$ and moves with constant volume flow rate $q_1 = \pi$, so that the velocity of the left-hand end of the gas slug is

$$\frac{\mathrm{d}x^{\text{l}}}{\mathrm{d}t} = \frac{q_1}{A(x^{\text{l}})}. \tag{8}$$

The second liquid slug occupies the region between x^{r} and the exit x_5. The volume flow rate of the slug is $q_2(t)$ and the liquid velocity $u(x) = q_2/A(x)$, so that

$$\frac{\mathrm{d}x^{\text{r}}}{\mathrm{d}t} = \frac{q_2(t)}{A(x^{\text{r}})}. \tag{9}$$

We define a velocity potential

$$\phi = \int_{x_5}^{x} \frac{q_2(t)}{A(x)}\,\mathrm{d}x. \tag{10}$$

The unsteady version of Bernoulli's equation leads to

$$\frac{\mathrm{d}q_2}{\mathrm{d}t}\int_{x_5}^{x^{\mathrm{r}}}\frac{\mathrm{d}x}{A(x)} = \frac{q_2^2}{2A^2(x_5)} - \frac{q_2^2}{2A^2(x^{\mathrm{r}})} + \frac{p_{\mathrm{exit}}}{\rho_{\mathrm{l}}} - \frac{p^{\mathrm{g}}}{\rho_{\mathrm{l}}} \tag{11}$$

with $q_2 = q_1$ initially. Thus we have four equations, Eqs. (7)–(9) and (11), for x^{l}, x^{r}, $q_2(t)$ and p^{g}.

We consider a Venturi with dimensions $x_1 = 4$, $x_2 = 5$, $x_3 = 6$, $x_4 = 7$, $x_5 = 11$. The equations were solved using the NAG routine D02CJF, a variable-order, variable-step Adams method and integration was stopped when the leading edge x^{r} of the gas slug reached the exit $x_5 = 11$. The leading edge of the gas slug was initially at $x^{\mathrm{r}} = 3$, unit distance away from the entrance to the Venturi at $x_1 = 4$. Therefore, deviations from steady flow commenced at time $t = 1$.

Initially the Venturi is filled with liquid and flow is steady. The non-dimensional pressure difference Δp_{l} between the entrance and throat of the Venturi is given by Bernoulli's theorem

$$\Delta p_{\mathrm{l}} = \frac{\beta^{-4} - 1}{2}, \tag{12}$$

so that $\Delta p_{\mathrm{l}} = 7.5$ when $\beta = 1/2$. If Δp_{l} is small compared to the initial pressure p_{exit} within the gas, the perturbed motion will be linear to a first approximation. Fig. 4 shows the pressure p^{g} within the gas slug as a function of time, with ambient pressure $p_{\mathrm{exit}} = 10^3$. The two curves correspond to slugs with initial length $L = 1.0$ and $L = 0.2$. The corresponding volumetric flow rates $q_2(t)$ are shown in Fig. 5.

Note that the frequency of the oscillations seen in Figs. 4 and 5 increases with time, since the inertia of the liquid between the slug and the exit decreases. The Venturi serves to excite

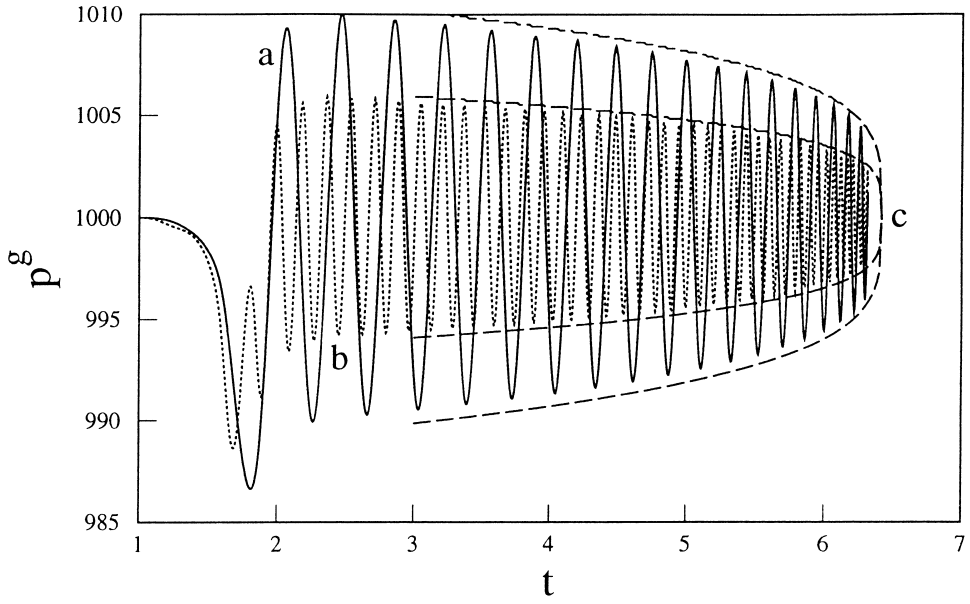

Fig. 4. The pressure p^{g} within the gas slug, as a function of time, for slugs with initial length (a) $L = 1.0$, (b) $L = 0.2$. Fixed exit pressure $p_{\mathrm{exit}} = 1000$. The envelopes (c) are proportional to $(t - t_0)^{1/4}$, where t_0 is the time at which the slugs reach the exit.

the oscillation, but plays little role once the gas has reached the uniform pipe beyond the constriction. The oscillations can therefore be analyzed by considering motion within a pipe of uniform cross-section with constant pressure p_{exit} applied at the exit x_5, and with a piston at $x^{\text{l}} = x_5 - U(t_0 - t) - L$ advancing towards the exit with constant velocity U. We suppose that there is a slug of gas in the region $x^{\text{l}} < x < x^{\text{r}}$ adjacent to the piston, and that liquid of density ρ_{l} occupies the remaining part of the tube $x^{\text{r}} < x < x_{\text{exit}}$. Thus, the geometry is similar to that shown in Fig. 2, but the pipe is now straight. Initially, the pressure is p_{exit} everywhere, the gas slug has length L, and piston, gas and liquid all move with velocity U, so that the gas slug will reach the exit x_5 at time $t = t_0$. The equation of motion for the liquid in $x^{\text{r}} < x < x^5$, Eq. (11), simplifies to

$$\ddot{x}^{\text{r}}\rho_{\text{l}}(x_5 - x^{\text{r}}) = p^{\text{g}} - p_{\text{exit}}, \tag{13}$$

where a dot represents differentiation with respect to time t. We look for a perturbation to steady motion in which the length $L + y$ of the gas slug oscillates slightly about L, and set

$$x^{\text{r}} = x_5 - L_{\text{l}} + y, \tag{14}$$

where L_{l} is the instantaneous (unperturbed) length of the oscillating column of liquid between the gas and the open end of the tube at x_5. The equation of motion, (13), becomes

$$\ddot{y}\rho_{\text{l}}(L_{\text{l}} - y) = -\frac{yp_{\text{exit}}}{L} + p_{\text{exit}}\left(\frac{y}{L}\right)^2 + \ldots, \tag{15}$$

with $|y| \ll L$. If $U = 0$ the unperturbed length L_{l} of the oscillating column of liquid is

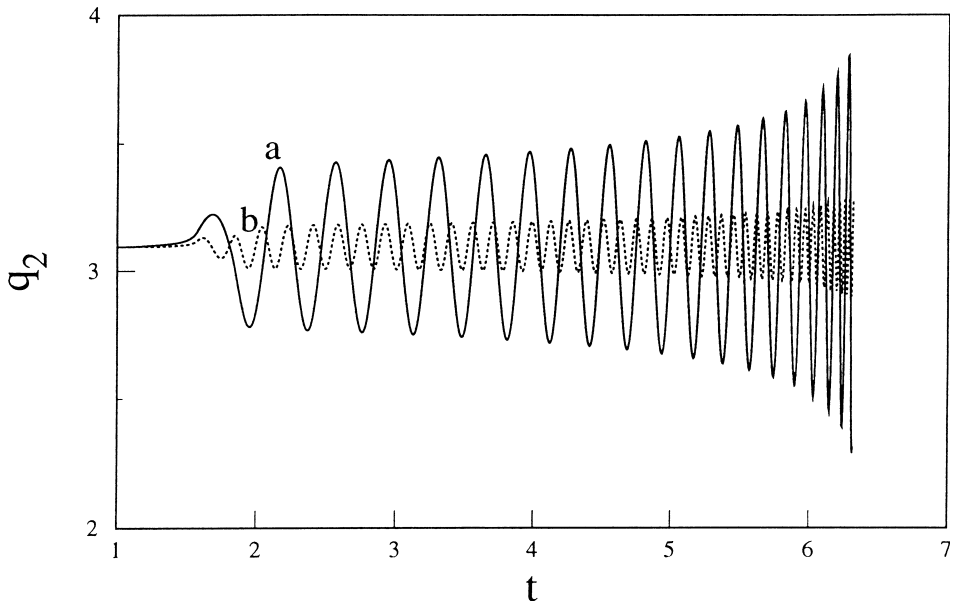

Fig. 5. The volume flow rate $q_2(t)$ within the liquid occupying the region $x_{\text{r}} < x < x_5$ for slugs with initial length (a) $L = 1.0$, (b) $L = 0.2$. Fixed exit pressure $p_{\text{exit}} = 1000$ (as in Fig. 4).

constant, and after neglecting terms $O(y/L)^2$ in Eq. (15) we find solutions of the form

$$y = a \sin \phi \tag{16}$$

where $\dot{\phi} = [p_{\text{exit}}/(LL_1\rho_1)]^{1/2}$ and a is constant. If $U \neq 0$ is sufficiently small such that L_1 varies little over one period of oscillation, we may still look for solutions of the form (16), with a varying slowly compared to ϕ. Setting $L_1 = U(t_0 - t)$, the equation of motion Eq. (15) becomes

$$\left[\left(\ddot{a} - a\dot{\phi}^2\right)\sin\phi + \left(2\dot{a}\dot{\phi} + a\ddot{\phi}\right)\cos\phi\right]\left[U(t_0 - t) - y\right] = -\frac{p_{\text{exit}}a}{\rho_1 L}\sin\phi + O(a/L)^2. \tag{17}$$

Equating terms in $\sin\phi$, to leading order we obtain

$$\dot{\phi} = \left(\frac{p_{\text{exit}}}{L\rho_1 U(t_0 - t)}\right)^{1/2} \tag{18}$$

and the frequency of the oscillation increases as the length of the liquid slug decreases. Equating terms in $\cos\phi$ to leading order gives

$$2\dot{a}\dot{\phi} + a\ddot{\phi} = 0 \tag{19}$$

and hence

$$a^2\dot{\phi} = \text{constant}. \tag{20}$$

As the frequency of oscillation $\dot{\phi}$ increases, the amplitude a decreases as $(t_0 - t)^{1/4}$. The dominant term of the perturbation velocity is $\dot{y} \simeq a\dot{\phi}\cos\phi$ and the amplitude of the velocity oscillations increases as $(t_0 - t)^{-1/4}$. Curves proportional to $(t_0 - t)^{1/4}$ are shown in Fig. 4, and are good fits to the envelopes of the oscillations.

If the ambient pressure is reduced to $p_{\text{exit}} = 10$, the oscillations of pressure within the gas become non-linear, with a much lower frequency and larger amplitude, as shown in Fig. 6.

A gas bubble occupies only part of the pipe, rather than the entire cross-section occupied by the slug, and is subject to interfacial tension. Nevertheless, calculations of bubble oscillations discussed in Section 5 exhibit similar features to the simple one-dimensional slug model presented above.

The model presented above could be extended in various ways. Thus one can study the motion of a train of N gas slugs by solving the corresponding $4N$ governing equations for the pressure, left- and right-hand coordinates of each gas slug and for the volume flow rates q_i of the intervening slugs of liquid. The resulting longitudinal oscillations are similar to those of a linear array of point masses connected by non-linear springs. The curvature of the interfaces could be allowed to vary, perhaps as a function of velocity, so that effects of surface tension could be included. We shall not discuss such extensions here.

3. Order of magnitude estimates for non-dimensional quantities

The range of flow rates which might be encountered when metering multiphase flow is large:

here we consider a dimensional flow rate $\tilde{q}_l = 10\ \mathrm{m}^3\ \mathrm{h}^{-1}$ such as might be achieved in a laboratory. If the pipe has radius $\tilde{a} = 25$ mm, the liquid velocity is $\tilde{U} = 1.4\ \mathrm{m\ s}^{-1}$. The liquid density is $\tilde{\rho}_l = 10^3\ \mathrm{kg\ m}^{-3}$, and a typical dynamic pressure is $\tilde{\rho}_l \tilde{U}^2 = 0.02$ bar. If the liquid is water with viscosity $\tilde{\mu} = 10^{-3}$ Pa s, the Reynolds number is $Re = 2\tilde{a}\tilde{U}\tilde{\rho}_l/\tilde{\mu} = 7 \times 10^4$. Thus, as stated above we expect the real flow to be turbulent. A typical interfacial tension for a clean air/water interface is $\tilde{\sigma} = 0.072\ \mathrm{N\ m}^{-1}$, so that the non-dimensional interfacial tension is

$$\sigma = \frac{\tilde{\sigma}}{\tilde{a}\tilde{\rho}_l \tilde{U}^2} = 1.5 \times 10^{-3}. \tag{21}$$

Note that σ defined by Eq. (21) is an inverse Weber number based on the radius of the pipe (rather than on that of the bubble).

A typical outlet pressure in the laboratory is 1 bar, and a typical inlet pressure is 2 bar. If we ignore interfacial tension, a typical non-dimensional initial bubble pressure is therefore $p_0^g = 100$. These pressures are large compared to the change in pressure within the throat of the Venturi, so that effects of bubble compressibility are small. More particularly, we would not expect to see the rapid growth of cavitation bubbles that occurs in cavitation susceptibility meters (Oldenziel, 1982). At a temperature 288 K the velocity of sound in air at atmospheric pressure is $340\ \mathrm{m\ s}^{-1} \gg \tilde{U}$ and the density of air $\tilde{\rho}_g = 1.2\ \mathrm{kg\ m}^{-3} \ll \tilde{\rho}_l$. We therefore ignore the inertia of the gas within the bubble, which we shall assume to be at uniform pressure.

We now consider the magnitude of the errors introduced by the neglect of gravity. In multiphase flowmeters the Venturi axis is usually vertical (Thorn et al., 1997) in order to maintain axisymmetry. The rise velocity of a Taylor bubble which spans a tube of diameter $2a$

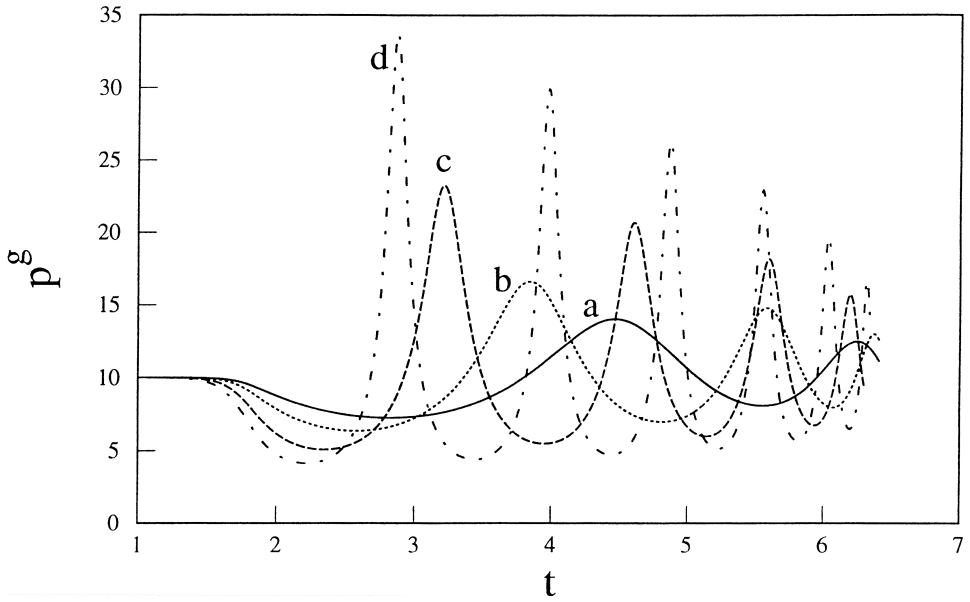

Fig. 6. As for Fig. 4, with exit pressure $p_{\mathrm{exit}} = 10$. Initial gas slug length (a) $L = 1.0$, (b) $L = 0.5$, (c) $L = 0.2$, (d) $L = 0.1$.

is approximately $0.48(ag)^{1/2}$ (Batchelor, 1973, p. 478) where g is the acceleration due to gravity. In a pipe of diameter 50 mm, this suggests a typical slip velocity 0.24 m s^{-1}. This is also the rate of rise of a bubble of radius approximately 0.5 mm in clean water, as predicted by the Levich formula and observed experimentally (Duineveld, 1995). The corresponding non-dimensional slip velocity is 0.2. Although this is not particularly small compared to the liquid velocity, it is small enough to justify an initial study of bubble motion in the absence of buoyancy.

A typical time taken for a bubble to pass through a Venturi of length 0.2 m will be of the order 0.1 s (the velocity within the Venturi is higher than that within the straight pipe). The thermal diffusivity of air at atmospheric pressure is typically 2×10^{-5} m^2 s^{-1}, so that thermal conduction will have time to equilibrate the temperature only within bubbles substantially smaller than 1 mm. In a turbulent churn-flow, mixing and heat transfer will be enhanced.

Kuo and Wallis (1988) performed experiments in which bubbles passed through a slot-shaped (as opposed to axisymmetric) nozzle, with an inlet velocity typically 0.8 m s^{-1}. The bubble diameters were typically 2 mm, compared to a throat cross-section 26 mm × 51 mm. These small bubbles survived their passage through the nozzle. Kuo and Wallis compared the bubble motion to the predictions of a one-dimensional model similar to that of Section 2.1, with additional viscous drag terms included. Agreement was good. The added mass force was important near the throat of the nozzle. Elsewhere drag and buoyancy forces dominated, as is inevitable in uniform sections of the pipe within which there is no acceleration. Fluctuations in differential pressure between the entrance and throat of the nozzle — not discussed by Kuo and Wallis — would have been small.

4. Boundary integral technique for potential flow

4.1. Green's identity

The liquid flow is assumed irrotational, so that the liquid velocity $\boldsymbol{u}$ may be represented by a potential ϕ such that

$$\boldsymbol{u} = \nabla\phi \tag{22}$$

where

$$\nabla^2\phi = 0 \tag{23}$$

because of incompressibility. The potential ϕ is obtained by solving the Laplace equation (23) at each time step by means of boundary integrals.

There have been a large number of numerical studies of bubble motion in potential flow based upon boundary integral techniques. Many of these concern cavitation bubbles, but gas bubbles were studied by Best and Kucera (1992), who included gravity but took interfacial tension to be zero. Other studies of gas bubbles rising under gravity include those of Lundgren and Mansour (1991), Boulton-Stone and Blake (1993) and Boulton-Stone et al. (1995). The

numerical method used here is based largely upon that described by Best and Kucera (1992) and Oguz and Prosperetti (1989, 1993).

To determine the liquid velocity $\boldsymbol{u}$ it is necessary to solve the Laplace equation (23) in the liquid domain Ω bounded by the surface S with outward facing normal $\boldsymbol{n}$. We shall adopt the method of solution based upon Green's second identity which leads to the integral equation for ϕ in the form

$$c\phi(x) = \int_S \left(\tilde{\phi} \frac{\partial \phi}{\partial n} - \phi \frac{\partial \tilde{\phi}}{\partial n} \right) \mathrm{d}S, \tag{24}$$

where $\tilde{\phi}$ is the fundamental solution; $c = 1$ for all points x within Ω, $c = 1/2$ if x lies on smooth portions of the boundary S, and $c = \alpha/2\pi$ if x lies at a corner of S at which the interior angle is α (Jaswon and Symm, 1977).

4.2. Discretisation of the boundary

Eq. (24) may be regarded as an integral equation. The boundary S of the liquid domain Ω consists of (i) the walls of the pipe, where we assume zero liquid velocity normal to the surface i.e. $\boldsymbol{n} \cdot \nabla\phi = \partial\phi/\partial n = 0$, (ii) the entrance to the pipe, on which we prescribe a non-dimensional normal velocity $U = 1$, (iii) the exit, on which we impose a constant pressure $p = p_{\mathrm{exit}}$, as a result of which ϕ is known, and (iv) the surface of the bubble, where the pressure and consequently ϕ are known.

The wall of the pipe is a simple, piecewise linear boundary and if we were prepared to take extra care when treating corners it would be possible to handle this boundary exactly. However, the liquid velocity $\boldsymbol{u} = \nabla\phi$ will be infinite at the corners C and D (Fig. 1). It was therefore decided to treat the wall as a smooth surface in similar fashion to the surface of the bubble. Typically 130 points were distributed along the wall and the axial and radial coordinates were interpolated by means of cubic splines (Press et al., 1992). Following Oguz and Prosperetti (1993), the rectilinear distance between points was used as the interpolating variable, rather than the curvilinear distance used by Best and Kucera (1992). The splines smooth out the corners over a lengthscale comparable to the discretisation used to represent the wall, so removing singularities at the corners. The entrance and exit to the pipe were represented by 11 points spaced regularly between the axis and the pipe wall. The bubble surface was usually described by 21 points, the first and last of which were on the pipe axis. If these were interpolated by cubic splines the computed curvature was found to be inaccurate, particularly at the points on the axis. Quintic splines were therefore used.

We assume that the unknown quantities (ϕ over the entrance and walls of the pipe; $\boldsymbol{n}\nabla\phi$ on the surface of the bubble and pipe exit) vary linearly with the spline parameter based on the linear distance between adjacent points.

When evaluating the surface integral in Eq. (24) all integrals in the θ direction were performed analytically in terms of complete elliptic integrals, for which efficient polynomial representations are available (Abramowitz and Stegun, 1964). The resulting line integrals were evaluated by means of a six-point Gauss–Legendre quadrature. Logarithmic terms were integrated by a procedure equivalent to that described by Oguz and Prosperetti (1993, Eq. (31).

In all the results presented here the dimensions of the Venturi were assumed to be $x_1 = x_5 - x_4 = 4.05$, $x_2 - x_1 = x_3 - x_2 = x_4 - x_3 = 1.0$. A more realistic Venturi for single phase flow would have a longer diverging section after the throat (British Standards Institution, 1997). There has been little discussion of optimal Venturi shapes for multiphase flow measurement.

4.3. Initial conditions

The Laplace equation was first solved in the absence of any bubble, assuming that the velocity normal to both the exit and entrance was U. The resulting Neumann problem can be solved only to within an arbitrary constant: this indeterminacy was removed by taking the potential at one point of the entrance to be zero. The potential ϕ was allowed to vary over the rest of the entrance, but in practice this was positioned sufficiently far upstream that the variation of ϕ across the entrance was negligible. The solution of the Neumann problem gives us an initial value for ϕ at the pipe exit.

The bubble was assumed to be initially spherical with centre at $x = 1$, sufficiently far upstream of the Venturi that the velocity potential could be taken to be $\phi = Ux$. This gives the initial condition for ϕ on the surface of a bubble moving at the same velocity U as the surrounding liquid.

In a real vertical Venturi the gas bubbles rise relative to the liquid because of buoyancy and in the computations the bubble could be given a different initial velocity. This was attempted, using the solution for potential flow around a sphere in unbounded liquid to give the initial potential on the surface of the bubble. The spherical bubble was not in equilibrium with the pressure over its surface; as a result the bubble not only translated, but also oscillated in shape. Such oscillations were reduced by taking the initial potential and bubble shape to be those of a perturbed sphere (Moore, 1959). However, oscillations were not entirely eliminated, no doubt because Moore considered bubbles in unbounded liquid, rather than within a pipe. We shall not pursue this further: from now on the initial velocity of the bubble will be equal to the velocity U of the surrounding liquid.

Initially the bubble is far upstream of the Venturi and the liquid surrounding the bubble is at the exit pressure p_{exit}. The bubble has radius R_0 and initial volume

$$V_0 = \frac{4}{3}\pi R_0^3. \tag{25}$$

The initial pressure within the bubble is

$$p_0^{\text{g}} = p_{\text{exit}} + \frac{2\sigma}{R_0}, \tag{26}$$

where σ is the non-dimensional interfacial tension.

4.4. Stepping forward in time

At the start of a time-step the potential ϕ and pressure p are known over the surface of the

bubble and over the exit. The tangential component of $\nabla\phi$ is therefore known, but the normal component must be determined by solving the integral equation (24). The surface of the bubble can then be translated, ready for the start of the next time step. The potential ϕ on the surface of the bubble and at the exit at the start of the next time-step are obtained via Bernoulli's equation

$$\frac{\partial\phi}{\partial t} + \tfrac{1}{2}u^2 + \tfrac{p}{\rho_1} = C(t), \tag{27}$$

where $u^2 = \boldsymbol{u}\cdot\boldsymbol{u}$ and $C(t)$ is constant along streamlines. In irrotational flow $C(t)$ may be taken to be the same on all streamlines: we choose $C = p_{\text{exit}} + \frac{1}{2}U^2$ so that the potential at the exit remains constant in the absence of any disturbance to the flow due to the presence of the bubble.

Integration forward in time was performed by a second-order Runge–Kutta scheme. Once the new position of the bubble surface has been determined, the new volume of the bubble and the corresponding gas pressure p^{g} within the bubble are computed. If the interfacial tension is σ, and R_1, R_2 are the principal radii of curvature of the surface, then the liquid pressure just outside the bubble is

$$p = p^{\text{g}} - \sigma\left(R_1^{-1} + R_2^{-1}\right). \tag{28}$$

A short wavelength, sawtooth instability has been encountered by many authors and is thought to be a numerical rather than physical instability. It was first reported by Longuet-Higgins and Cokelet (1976), who suppressed it by means of a smoothing procedure. Lundgren and Mansour (1988) smoothed it by means of a diffusion step

$$\frac{\partial\psi}{\partial t} = -\lambda\frac{\partial^4\psi}{\partial s^4}, \tag{29}$$

where ψ is the quantity to be smoothed, and λ controls the degree of smoothing. The smoothed value of ψ is

$$\psi_j' = \psi_j - \frac{\lambda\Delta t}{(\Delta s)^4}\left[\psi_{j+2} - 4\psi_{j+1} + 6\psi_j - 4\psi_{j-1} + \psi_{j-2}\right], \tag{30}$$

where Δs is the distance between grid points, and Δt is the length of the diffusion time step. Lundgren and Mansour took $\lambda_1 = \lambda\Delta t/(\Delta s)^4 = 0.01$. If $\lambda_1 = 1/16$, Eq. (30) is equivalent to the five-point formula of Longuet-Higgins and Cokelet (1976). The various instabilities are discussed by Dold (1992). In the results presented here the five-point smoothing algorithm of Longuet-Higgins and Cokelet (1976) was applied every 200 time steps. At each time step the points representing the bubble were re-distributed in order to maintain an approximately even spacing. The time step was typically chosen initially to be $\Delta t = 10^{-4}$ but was reduced by a factor 5 when the bubble entered the Venturi.

4.5. Pressures

We evaluate all pressures in the liquid relative to the pressure p_{exit}. Once the potential ϕ has

been obtained along the walls of the pipe, it is fitted by splines and can be differentiated in order to determine the liquid velocity at the wall. The time derivative $\partial\phi/\partial t$ may be estimated as a backward derivative using the value of ϕ at the previous time step. The wall pressure p is then determined by means of Bernoulli's equation, (27). In an experiment the wall pressure would be measured at a series of pressure tappings: in the numerical computations the pressure was computed at the start and end of the converging section (B and C in Fig. 1), at the start and end of the diverging section (D and E in Fig. 1), at the midpoint of the Venturi throat, and at non-dimensional distances 1 upstream of B and downstream of E. We identify these pressures as $p_1, \ldots, p_7$, as shown in Fig. 1. The entrance pressure p_{in} was also noted.

If the bubble volume changes from V_0 to V the (isothermal) gas pressure becomes

$$p^{\text{g}} = \frac{p_0^{\text{g}} V_0}{V} \tag{31}$$

$$= p_0^{\text{g}} + p_{\text{bub}}, \tag{32}$$

where

$$p_{\text{bub}} = M\left(\frac{1}{V} - \frac{1}{V_0}\right) \tag{33}$$

is the perturbation to the gas pressure within the bubble and

$$M = p_0^{\text{g}} V_0. \tag{34}$$

In equilibrium, the radius R_0 of a spherical bubble satisfies

$$p_{\text{exit}} = \frac{3M}{4\pi R_0^3} - \frac{2\sigma}{R_0}, \tag{35}$$

so that

$$\frac{\mathrm{d}R_0}{\mathrm{d}p_{\text{exit}}} = -\left[\frac{9M}{4\pi R_0^4} - \frac{2\sigma}{R_0^2}\right]^{-1}. \tag{36}$$

We shall generally investigate values of $\sigma \ll 9M/8\pi R_0^2$, so that interfacial tension plays little role in determining the volume of the bubble as it passes through the Venturi. However, it will play an important role in determining perturbations from a spherical shape.

The derivative $\mathrm{d}R_0/\mathrm{d}p_{\text{exit}}$ in Eq. (36) is singular when $\sigma = 9M/8\pi R_0^2$. The non-dimensional frequency of small oscillations of a bubble in unbounded liquid is (e.g. Leighton, 1994, p. 183)

$$\omega_0 = \frac{1}{R_0}\left[3p_0^{\text{g}} - \frac{2\sigma}{R_0}\right]^{1/2}. \tag{37}$$

Thus we expect instability if $M < 8\pi R_0^2\sigma/9$. This corresponds to a negative ambient pressure $p_{\text{exit}} < -4\sigma/(3R_0)$.

4.6. Code validation

The Neumann problem in Section 4.3 was first solved in order to determine ϕ at the exit in the absence of any bubble. The results can also be used to obtain the liquid velocity on the centreline and wall, and the corresponding pressures. These are shown in Figs. 7 and 8 for the case $\beta = 1/2$. The velocity at the corners C and D of the Venturi throat is large but finite: the singularity has been removed by the smoothing of the corners. The volumetric flow rate obtained by integrating the liquid velocity across the pipe section was least accurate near these corners, but even here errors were less than 1%. Note that the wall and centreline velocities differ slightly even at the centre of this unrealistically short Venturi.

If $\beta = 1$ the pipe is straight, and it is straightforward to check that the bubble translates without deformation. The code can be used to predict the frequency of a monopole oscillation of a bubble, and the numerical results are in good agreement with analytic predictions, as discussed in Appendix A.

The code did not always run successfully. Thus, very small bubbles, which should be stable, required small time steps and such bubbles had to travel many bubble diameters in order to pass through the Venturi. Large bubbles proved to be unstable, particularly when they came close to the wall. The success of simulations of a deforming droplet (Tsai and Miksis, 1994) or capsule (Leyrat-Maurin and Barthès-Biesel, 1994) at zero Reynolds number may in part be because viscosity slows down the rate of approach to the wall, thereby making the problem more stable. Although large gas slugs can

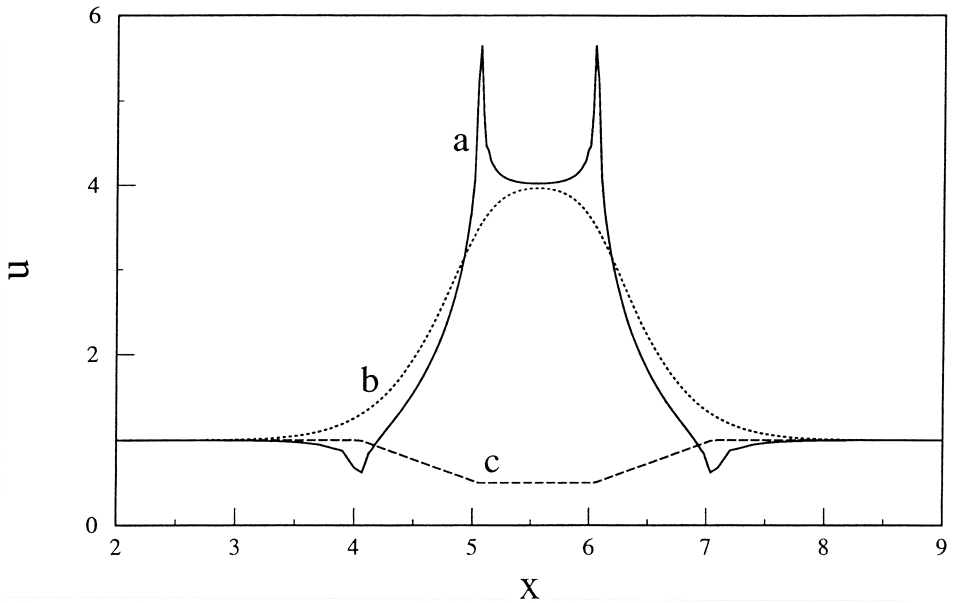

Fig. 7. The non-dimensional liquid velocity (a) at the wall, and (b) along the centerline. Curve (c) shows the non-dimensional radius of the Venturi with $\beta = 1/2$.

propagate steadily in a straight pipe at high Reynolds number, the behaviour of the film of liquid at the wall is generally thought to be governed by a balance between viscous and gravitational forces, both of which have been neglected here. Udaykumar et al. (1997) computed the motion of a droplet of low (but non-zero) viscosity through a constriction at Reynolds number 50. They successfully followed the drop to larger deformations than were achieved here, though their simulations also eventually failed, especially if the droplet touched the walls of the Venturi.

Tests were performed to check that the chosen time step was sufficiently small. The example of a Venturi with $\beta = 0.9$ and a bubble of radius $R_0 = 0.5$ with interfacial tension $\sigma = 0.1$ will be discussed in detail in Section 5.1 (Figs. 10 and 14). For this case a reduction of the time-step from 2×10^{-5} to 4×10^{-6} changed the position of the centre of mass of the bubble at time $t = 9$ by less than 0.001. Similarly, we may change the number of points used to represent the surface of the bubble, and we examine the case $\beta = 0.8$, $R_0 = 0.5$, $\sigma = 0.2$, $M = 100$ considered in Section 5.3 (Fig. 21) for which the numerical code failed shortly after time $t = 7.5$. Thus, resolution problems were worse than usual in this example. The broken lines in Fig. 9 show bubbles represented by 21 points marked by open circles. Solid lines indicate bubbles represented by 41 points. In both cases the time step was 2×10^{-5}. Only half of each axisymmetric bubble is shown, at times $t = 5.0$, 5.5, 6.0, 6.5 and 7.0. The radial and axial scales are different: results at these and other times will be shown in Fig. 21 with correct scaling. We see that differences between the two resolutions are small up to $t = 5.5$. By $t = 6.0$ discrepancies begin to occur, but the bubble is by now well past the throat of

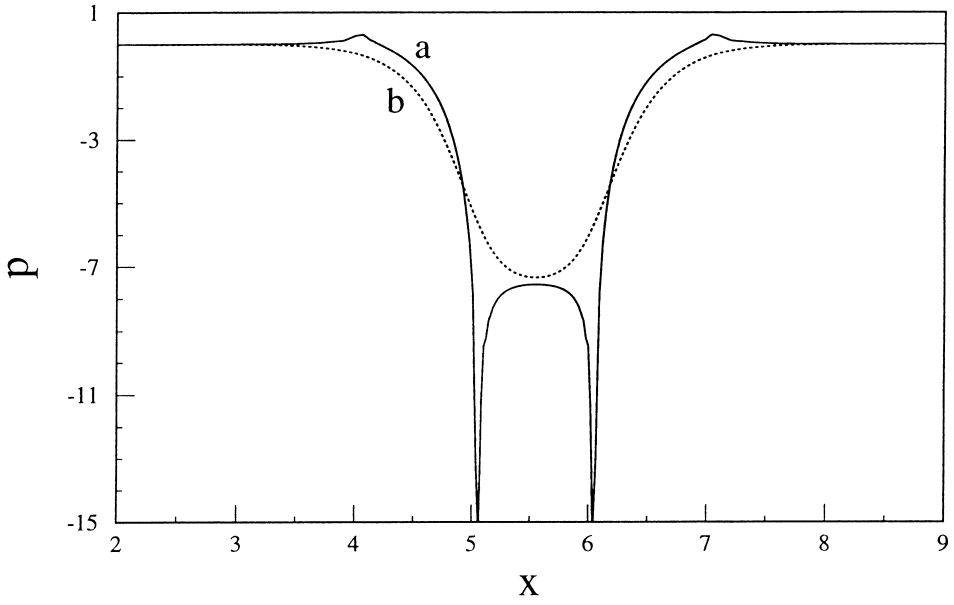

Fig. 8. The non-dimensional pressure p, relative to the pressure p_{exit} (a) along the wall, (b) along the centerline. Throat radius $\beta = 1/2$, as in Fig. 7.

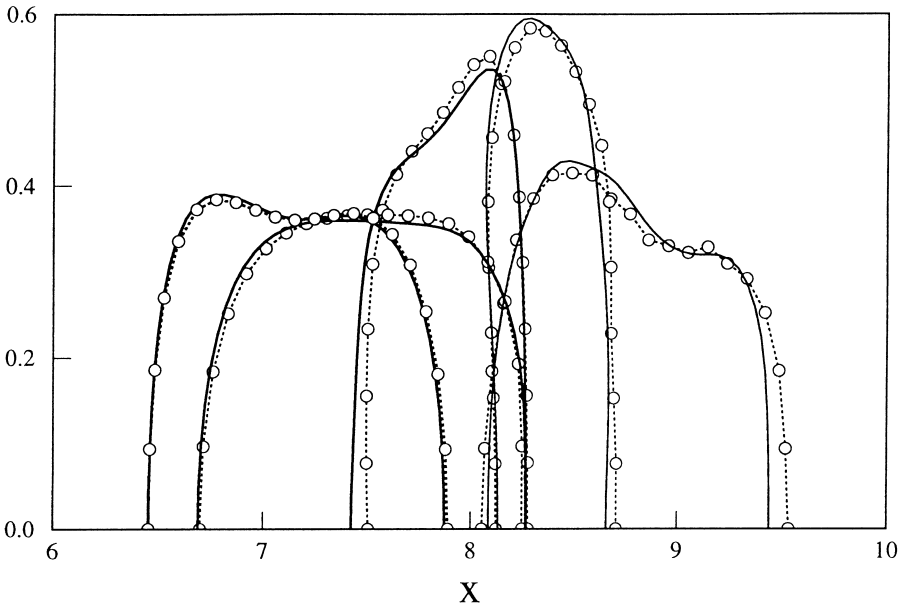

Fig. 9. Computed bubble shapes for the case $\beta = 0.8$, $R_0 = 0.5$, $\sigma = 0.2$, $M = 100$ at times t = 5.0, [0.5], 7.0, ——— using 41 points to represent the bubble; ···○··· using 21 points. Further results for this case are shown, correctly scaled, in Fig. 21.

the Venturi. The discrepancies eventually become large at $t = 7.5$ shortly before the code failed (in both cases).

5. Results

5.1. Motion of a bubble in a Venturi with throat radius $\beta = 0.9$

The one-dimensional analysis of Section 2.1 assumed that the added mass of the bubble remained constant. This is untrue in a Venturi, since the added mass of a sphere in a tube depends upon the ratio of the diameter of the tube to that of the sphere (Smythe, 1961; Cai and Wallis, 1992). In order to compare the results of the boundary integral computations with those of the one-dimensional model, we first consider a Venturi with throat radius $\beta = 0.9$, for which the added mass of the bubble varies little between the entrance and the throat. The choice $\beta = 0.9$ has the additional advantage of ensuring that the bubble deformation is small. The Venturi considered in this paper is short and when $\beta = 0.5$ large bubbles deformed so much on entering the rapidly converging section of the Venturi that the numerical scheme failed. We shall restrict our attention to a limited range of the interfacial tension σ. If $\sigma \ll 1$, the bubble deforms rapidly and breaks. If $\sigma \gg 1$, the bubble stays approximately spherical, and oscillations are largely suppressed.

We first consider a bubble of radius $R_0 = 0.5$ with surface tension $\sigma = 0.1$, which although

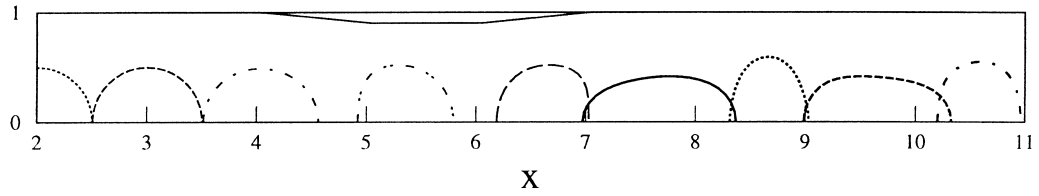

Fig. 10. The deformation of a bubble with initial radius $R_0 = 0.5$ as it passes through a Venturi with $\beta = 0.9$, at times $t = 1$, [1], 9. $M = 100$, $\sigma = 0.1$.

small is not as small as the typical experimental values estimated in Section 3. We take $M = 100$ corresponding to $p_0^g = 191$. Fig. 10 shows a series of deformed bubble shapes caused by passage through the Venturi and Fig. 11 shows a more detailed plot of the deformation. There is a quadrupole oscillation with a period approximately 2. The frequency $\tilde{\omega}_n$ of an nth order spherical harmonic perturbation to a spherical bubble is given by Lamb (1932, p. 475):

$$\tilde{\omega}_n^2 = (n+1)(n-1)(n+2)\frac{\tilde{\sigma}}{\tilde{\rho}_1 \tilde{R}_0^3}. \tag{38}$$

Hence, for a quadrupole ($n = 2$) the non-dimensional frequency

$$\omega_2 = \left(\frac{12\sigma}{R_0^3}\right)^{1/2}, \tag{39}$$

and the predicted period is $2\pi/\omega_2 = 2.03$, in good agreement with that observed in the simulation. The disturbance velocity falls off relatively rapidly away from a quadrupole, and it is therefore not surprising that the frequency has hardly been affected by the presence of the pipe walls.

Fig. 12 shows the pressure at the inlet and the change in pressure p_{bub} (33) within the bubble. When the bubble enters the Venturi then gas, rather than liquid, is being accelerated and the

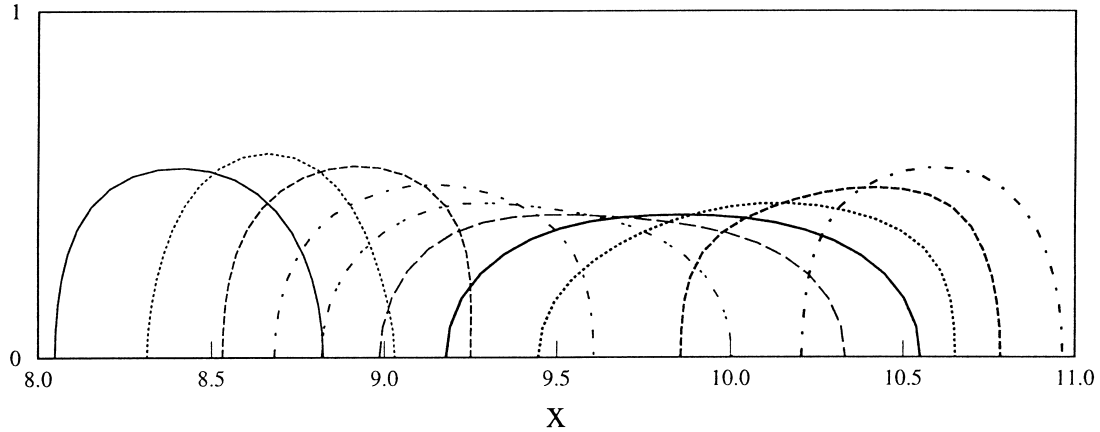

Fig. 11. Detail of Fig. 10, at times $t = 6.75$, [0.25], 9.0.

pressure at the entrance decreases from its initial value 0 (relative to p_{exit}). There is a corresponding increase in the inlet pressure when the bubble leaves the Venturi.

In single-phase flow the pressure at the centre of the Venturi is expected, by Eq. (12), to be $p_4 = -0.26$ and we see in Fig. 12 that the perturbation pressure within the bubble approximately attains this value. The monopole mode of oscillation of the compressible bubble is also excited by passage through the Venturi. The frequency in unbounded liquid predicted by Eq. (37) is $\omega_0 = 47.9$ with a period $2\pi/\omega_0 = 0.13$. The frequency of oscillation seen in Fig. 12 is lower and increases with time; this is reminiscent of results from the one-dimensional slug model of Section 2.2. The predictions of this model for the change in pressure within a gas slug of volume equal to that of a sphere of radius $R_0 = 0.5$, at an exit pressure $p_{\text{exit}} = 191$, are shown in Fig. 13 for a Venturi with $\beta = 0.9$. Also shown is the change in pressure of the bubble (as in Fig. 12). The frequencies and magnitudes of the perturbed pressures within the slug and bubble are similar, though that in the bubble is modulated by other frequencies. In Appendix A we discuss how the frequency of monopole oscillations of a bubble in a straight pipe differs from that in unbounded liquid.

Fig. 14 shows the wall pressures $p_1, \ldots, p_7$ at positions discussed in Section 4.5 and shown in Fig. 1. We see that the wall pressure at any particular position changes little while the bubble is upstream, since the pressure at the exit is held constant. The wall pressure subsequently oscillates once the oscillating bubble has passed by. However, pressure differences are not affected by this oscillation. In Fig. 15 we see the differential pressure $\Delta p = p_1 - p_4$, both for the example of Fig. 10 with $\sigma = 0.1$, and for a second case in which $\sigma = 1.0$. In both cases, Δp decreases as the bubble enters the Venturi: it is easier to accelerate gas than liquid. There is then an increase to a level which is higher than that for flow of liquid alone. The reason for

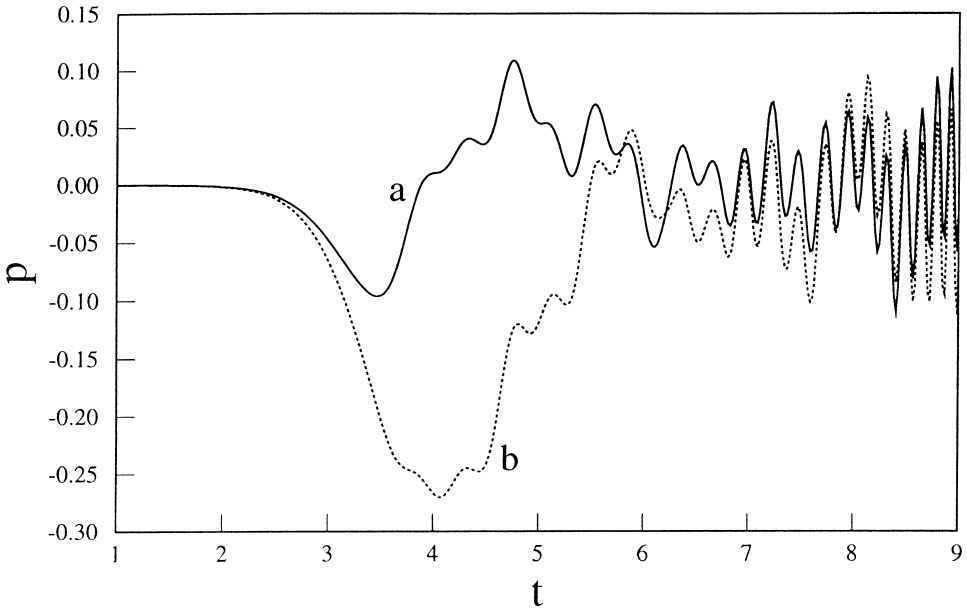

Fig. 12. Pressures computed during the simulation of Fig. 10. (a) Entrance pressure p_{in}, (b) change in bubble pressure p_{bub}. $M = 100$, $\sigma = 0.1$, $\beta = 0.9$.

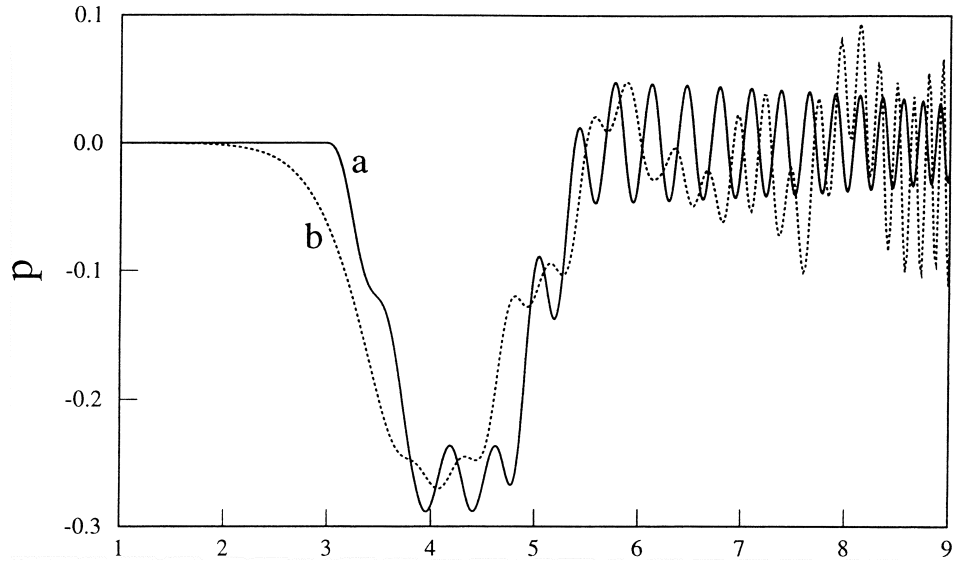

Fig. 13. (a) The change in slug pressure computed by the one-dimensional model of Section 2.2, for a slug with volume equal to that of a bubble of radius $R_0 = 0.5$, with exit pressure $p_0 = 191.0$. (b) Change in bubble pressure p_{bub} computed during the simulation of Fig. 10. $\sigma = 0.1$, $\beta = 0.9$, $M = 100$, $R_0 = 0.5$.

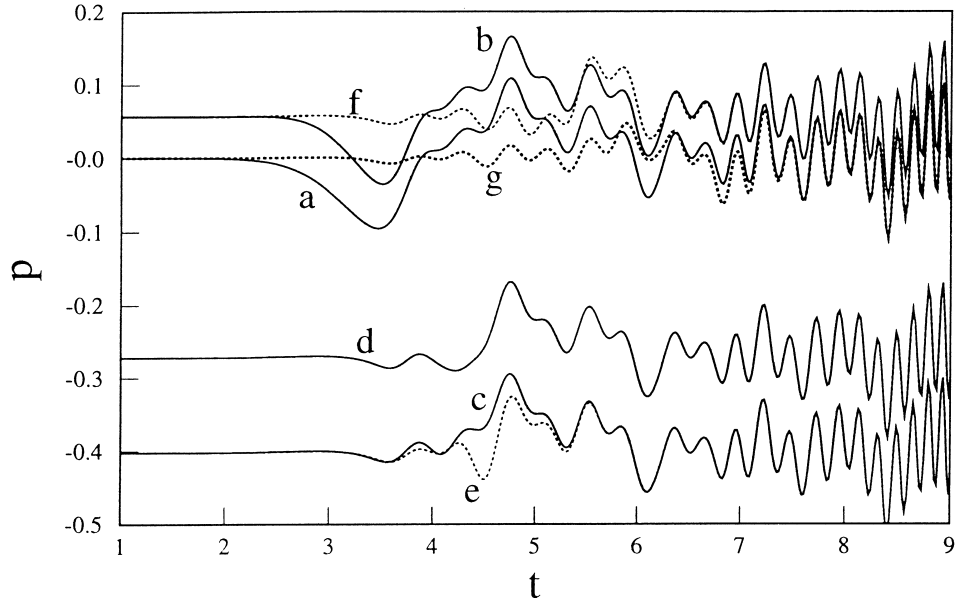

Fig. 14. Wall pressures computed during the simulation of Fig. 10. (a) p_1, (b) p_2, (c) p_3, (d) p_4 (the mid-point of the throat), (e) p_5, (f) p_6, (g) p_7.

the re-bound of Δp is straightforward. At the centre of the Venturi the bubble is travelling faster than the surrounding liquid. Consider a bubble travelling at constant velocity in a straight pipe, as seen in the frame of reference moving with the bubble, so that the velocity field is steady. The liquid velocity at the wall is higher in the neighbourhood of the bubble than either up- or down-stream. This leads to a decrease in wall pressure near the bubble and hence to an increase in Δp as the bubble passes the centre of the throat, where the wall pressure is computed. There is no equivalent effect when the bubble passes the position upstream of the throat at which the pressure is computed, as here the bubble has the same velocity as the surrounding liquid. The fine details of the pressure pulse as the bubble passes through the throat will depend upon the shape and velocity of the bubble, which are modified by changes in the interfacial tension and bubble compressibility.

Note that in Fig. 15 the differential pressure measured in the absence of the bubble is $\Delta p_l = 0.273$, rather than 0.262 as predicted by Eq. (12). The discrepancies between single phase potential flow computations and the results of one-dimensional models were discussed in Section 4.6.

The results of Figs. 12–15 were plotted as functions of time t. In order to help interpret them in terms of the position of the bubble, we show in Fig. 16 the position of the centre of mass of the bubble as a function of time as seen by an observer moving with velocity $u = 1$ along the x direction. Also shown are the positions of the intersections of the bubble surface with the centreline, at the front and back of the bubble. The oscillations in these latter curves are caused by the quadrupole oscillation of the bubble. Also shown in Fig. 16 is the position $x_b(t)$ of the centre of a spherical bubble as predicted by the one-dimensional model of Section 2.1, corresponding to Eqs. (4) and (5) with $u_l = R_p^{-2}$ and added mass coefficient $C_m = 1/2$.

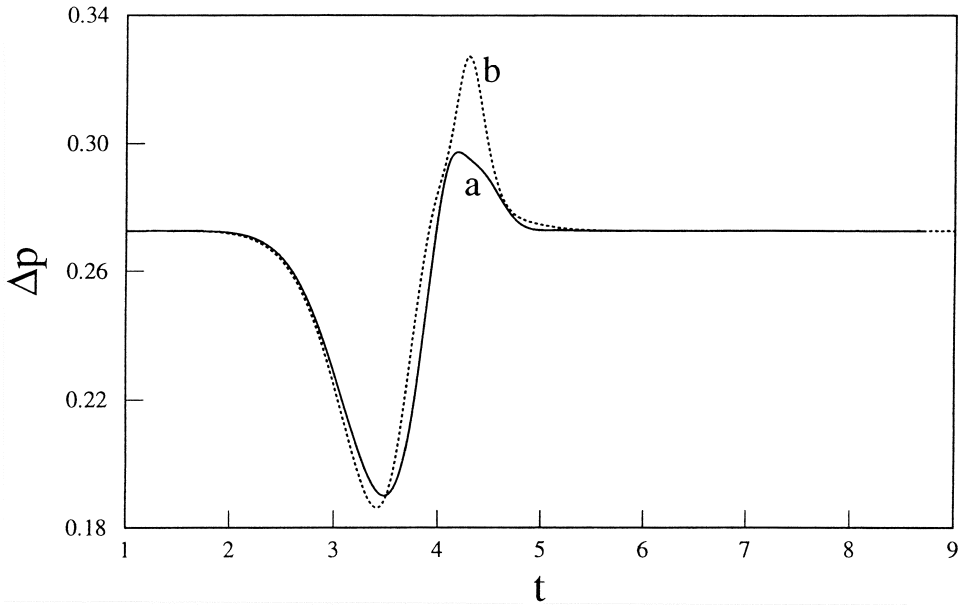

Fig. 15. The differential pressure Δp in a simple Venturi with $\beta = 0.9$, during the passage of a bubble with initial radius $R_0 = 0.5$. Interfacial tension (a) $\sigma = 1.0$; (b) $\sigma = 0.1$. $M = 100$.

When the oscillating bubble emerges from the Venturi, it has a lower velocity than the liquid. This is perfectly possible in potential theory, though in reality viscous drag at the surface of the bubble would ensure (in the absence of gravitational effects) that the bubble eventually regains the velocity of the surrounding liquid. It is well established that self-propulsion of a deformable body in an irrotational inviscid fluid can be achieved by changes of body shape (Saffman, 1967; Miloh and Galper, 1993; Galper and Miloh, 1995).

5.2. The effect of interfacial tension

We now consider the effect of raising the interfacial tension from $\sigma = 0.1$ to $\sigma = 1.0$, while keeping all other variables constant ($\beta = 0.9$, $M = 100$, $R_0 = 0.5$). A plot similar to Fig. 10 would show the bubble passing through the Venturi with almost no deformation. The position of the bubble is shown as a function of time in Fig. 17(a). The bubble emerges from the Venturi with the same velocity as that of the liquid.

The predictions of the one-dimensional model of Section 2.1 are shown in Fig. 17(b), assuming $u_l = R_p^{-2}$ and $C_m = 1/2$. Note that the full numerical computation predicts that the bubble starts to accelerate sooner than predicted by the one-dimensional model. This is because the irrotational liquid velocity u_l on the centreline accelerates upstream of the converging section, as seen in Fig. 7. The one-dimensional model, given by Eq. (4), can be integrated using the irrotational velocity u_l rather than the approximation of Eq. (5), and this leads to curve (d) when $C_m = 1/2$. Taking $C_m = 0.667$, corresponding to a sphere of radius $R_0 = 0.5$ in a straight pipe (Smythe, 1961), we predict Fig. 17(c). The added mass of the sphere

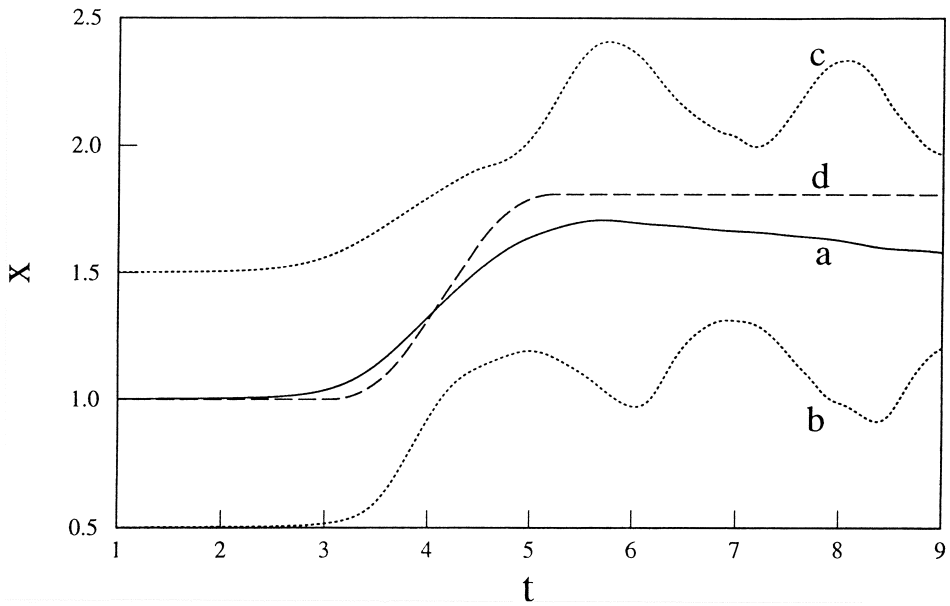

Fig. 16. The position of the bubble of Fig. 10, as seen by an observer moving with constant velocity $u = 1$. (a) Centre-of-mass of the bubble; (b) and (c) show the trailing and leading edges of the bubble on the pipe axis; (d) the prediction of the one-dimemsional model of Section 2.1, with $C_m = 1/2$ and $u_l = R_p^{-2}$. $M = 100$, $\sigma = 0.1$, $\beta = 0.9$.

will increase within the throat, where the ratio of the bubble diameter to pipe diameter increases to 0.555. Nevertheless this increase is too small to affect the agreement between the full results and those of the one-dimensional model with C_m constant. Thus we have shown that the simple one-dimensional model of Section 2.1 can predict the motion of the bubble, as long as (i) the liquid velocity is obtained from a full solution of potential flow, rather than by assuming a uniform velocity across the cross-section, (ii) the effect of the pipe is considered when choosing a value for the added mass coefficient C_m, and (iii) the bubble remains spherical. If the bubble is sufficiently small it will remain spherical due to surface tension, and its added mass coefficient will differ little from the value $C_m = 1/2$ in unbounded fluid.

Fig. 18 shows the variation of the bubble volume as a function of time for the two cases $\sigma = 0.1$ and $\sigma = 1.0$. If the bubble remained spherical, Eq. (36) implies that at a pressure $p_0^g = 191$ (corresponding to $M = 100$) the variation in σ should make little difference to the radius of the bubble. We see in Fig. 18 that this holds for the slow changes in pressure associated with motion into the low pressure region at the throat of the Venturi. The main effect of an increase in surface tension is to suppress the quadrupole oscillation, but this has the indirect effect of suppressing any excitation of the monopole. Longuet-Higgins (1989a, 1989b) has shown that if a bubble is deformed without change in volume, energy can be transferred from the higher multipole deformations to excite a second-order (but potentially non-negligible) monopole oscillation at a frequency twice that of the multipole. This is discussed further by Benjamin (1989) and Longuet-Higgins (1989c, 1991). Previous work concerns bubbles in unbounded fluid; the effect of the pipe walls is unknown and possibly enhances the coupling.

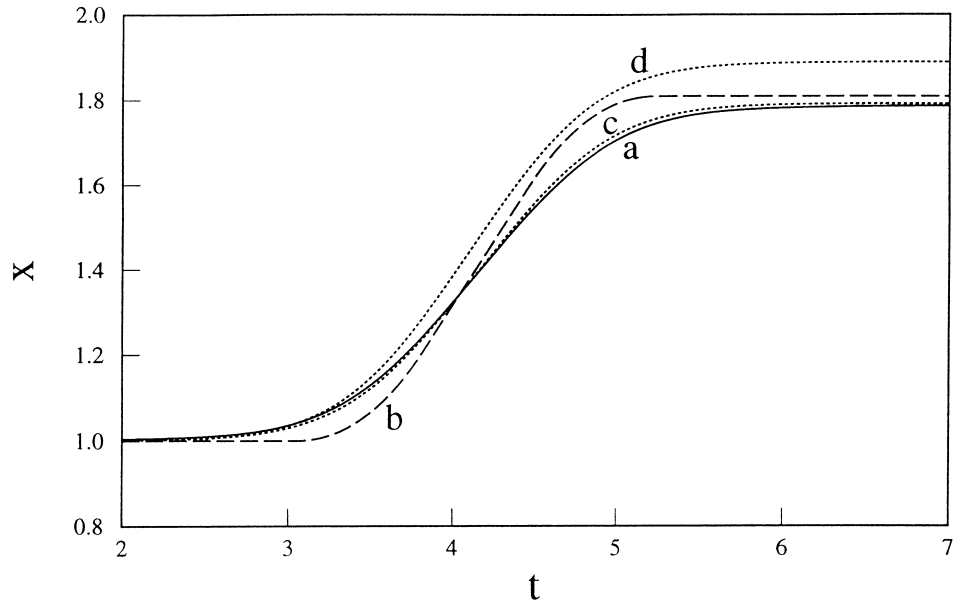

Fig. 17. Results similar to Fig. 16, for interfacial tension $\sigma = 1.0$. (a) Centre-of-mass of the bubble; (b) prediction of the one-dimensional model of Section 2.1 with $C_m = 1/2$ and $u_l = R_p^{-2}$ (c) one-dimensional model with $C_m = 0.667$ and inviscid potential potential flow u_l; (d) one-dimensional model with $C_m = 1/2$ and inviscid potential flow u_l.

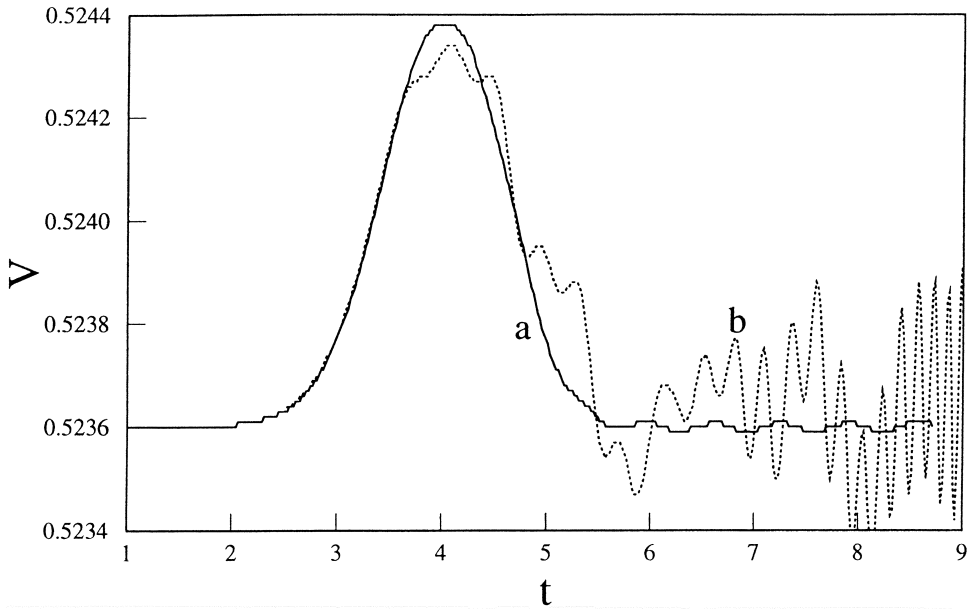

Fig. 18. The bubble volume V during passage through a Venturi with $\beta = 0.9$. Interfacial tension (a) $\sigma = 1.0$; (b) $\sigma = 0.1$. $M = 100$. $R_0 = 0.5$.

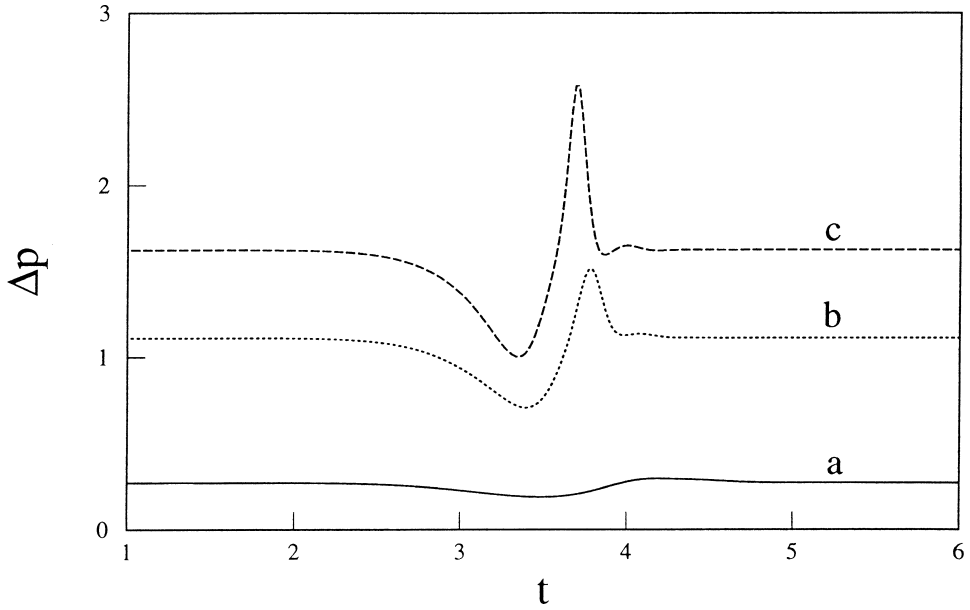

Fig. 19. The differential pressure $\Delta p = p_1 - p_4$, for (a) $\beta = 0.9$; (b) $\beta = 0.75$; (c) $\beta = 0.7$. $\sigma = 1.0$, $M = 100$, $R_0 = 0.5$.

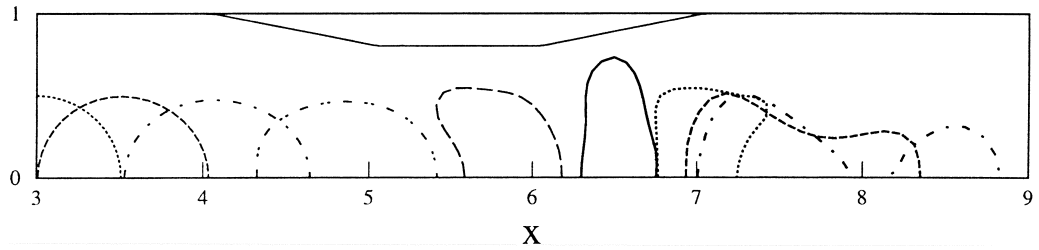

Fig. 20. The deformation of a bubble with initial radius $R_0 = 0.5$ as it passes through a Venturi with $\beta = 0.8$, at times $t = 2.0$, [0.5], 5.5, 5.73. $M = 100$, $\sigma = 0.1$.

5.3. The effect of Venturi throat diameter β

In Fig. 19 we see the differential pressure $\Delta p = p_1 - p_4$ for a bubble of radius $R_0 = 0.5$ with $M = 100$ and with interfacial tension $\sigma = 1.0$ passing through Venturis with $\beta = 0.9$, 0.75 and 0.7. As expected, the perturbation to the differential pressure increases as β decreases. Note also that the bubble passes more quickly through the narrower Venturis.

When $\sigma = 1.0$ the bubble did not survive its passage through a Venturi with throat radius $\beta = 0.6$. Fig. 20 shows the case $\beta = 0.8$, $\sigma = 0.1$. The bubble becomes elongated and snaps at its centre. If surface tension is increased to $\sigma = 0.2$, as shown in Fig. 21, the numerical scheme is eventually unable to follow the distorted shape of the bubble. Udaykumar et al. (1997) used a mixed Eulerian–Lagrangian code to compute the motion of a droplet through a constriction at Reynolds number 50, and the distortion shown in Fig. 21 is similar to the early stages of droplet breakup predicted in some cases by their computations once the drop has emerged from the constriction.

Fig. 22 shows the change in bubble pressure, p_{bub}, as given by Eq. (33). We see that when $\beta = 0.9$ the Venturi is too weak to excite any significant change in the volume of the bubble, unlike the narrower Venturi with $\beta = 0.7$. Note the smoothly varying envelope which modulates the pressure fluctuations within the bubble.

5.4. The effect of bubble compressibility and absolute pressure

When the ambient pressure is decreased, the change in pressure as the bubble passes through the Venturi will have a greater effect on the bubble, i.e. the gas becomes more compressible.

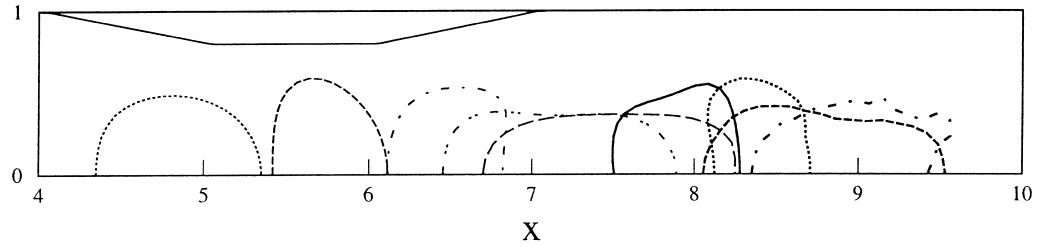

Fig. 21. The deformation of a bubble with initial radius $R_0 = 0.5$ as it passes through a Venturi with $\beta = 0.8$ at times $t = 3.5$, [0.5], 7.5. $M = 100$, $\sigma = 0.2$.

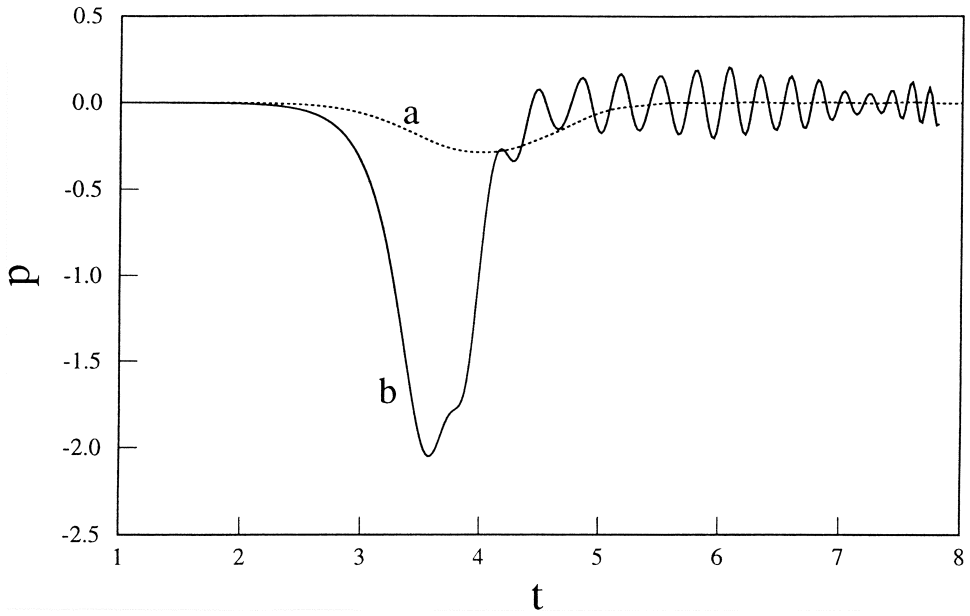

Fig. 22. The perturbation pressure p_{bub} within the bubble, as a function of time. $\sigma = 1.0$. $M = 100$, $R_0 = 0.5$. (a) $\beta = 0.9$, (b) $\beta = 0.7$.

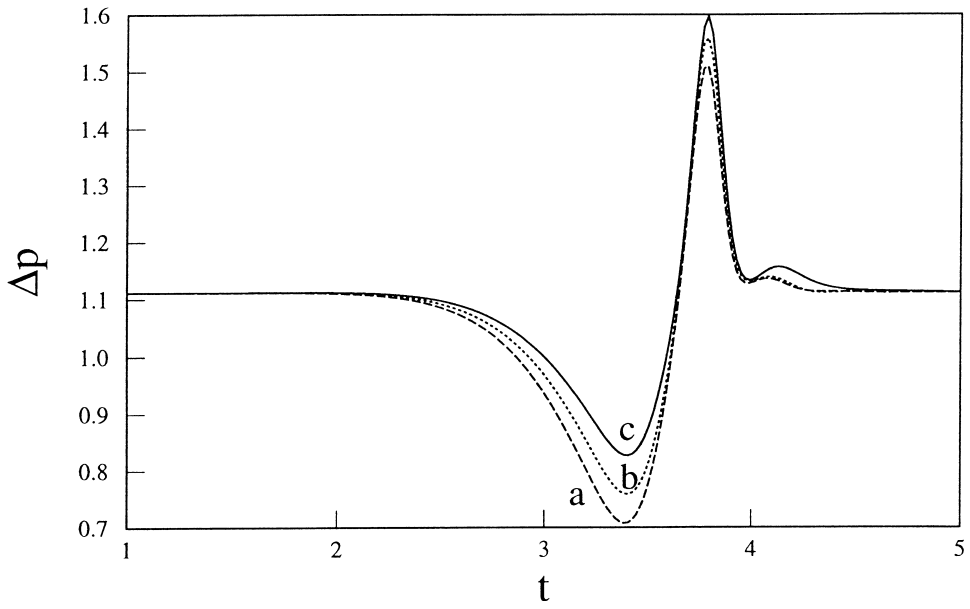

Fig. 23. The effect of changes in ambient pressure on the differential pressure Δp during the passage of a bubble. Bubble radius $R_0 = 0.5$, interfacial tension $\sigma = 1.0$, Venturi throat radius $\beta = 0.75$. (a) $p_0^g V_0 = M = 100$, (b) $M = 10$, (c) $M = 1.0$.

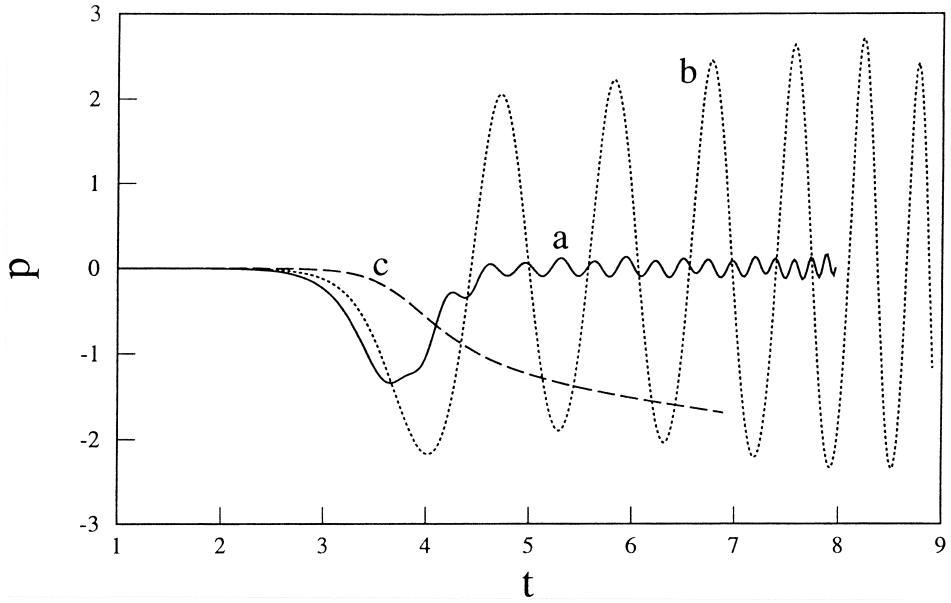

Fig. 24. The perturbation pressure p_{bub} within bubbles with $\sigma = 1$ passing through a Venturi with $\beta = 0.75$. (a) $M = 100$, (b) $M = 10$, (c) $M = 1.0$.

Fig. 23 shows Δp when a bubble of radius $R_0 = 0.5$ with interfacial tension $\sigma = 1.0$ passes through a Venturi with $\beta = 0.75$. When $M = p_0^{\text{g}} V_0$ is decreased, the bubble becomes more compressible and expands more when it enters the low-pressure region of the Venturi throat. This increases the total volumetric flow rate at the throat and tends to increase Δp.

Fig. 24 shows the perturbation p_{bub} of Eq. (33), to the pressure within the bubbles of Fig. 23. When M is large the bubble oscillates little. The oscillations grow in amplitude and decrease in frequency as M decreases. Similar behaviour was seen in the one-dimensional slug model of Section 2.2. When $M = 1.0$ the initial pressure within the bubble is $p_0^{\text{g}} = 1.91$, and we see that $p^{\text{g}} \rightarrow 0$ as t increases. The bubble is expanding without limit. This growth can be seen in Fig. 25, which shows the deformation of the bubble as it passes through the Venturi. From Eq. (36) we

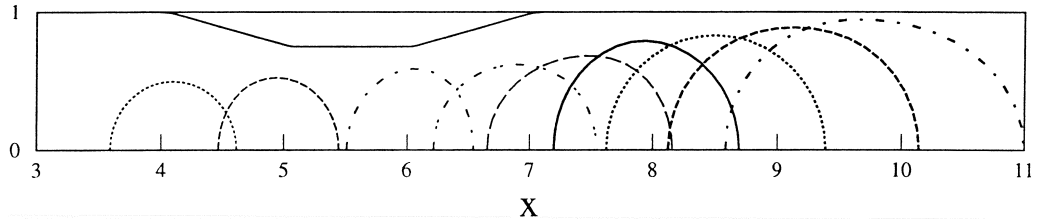

Fig. 25. The deformation of a bubble with initial radius $R_0 = 0.5$ as it passes through a Venturi with $\beta = 0.75$, at times $t = 3$, [0.5], 6.5, 6.89. $M = 1.0$, $\sigma = 1.0$.

note that if the bubble were in unbounded liquid it would only have to grow in radius from 0.5 to 0.6 to become unstable, and then to grow without limit. The continued expansion of the bubble in Fig. 25 is similar to critical flow of a gas–liquid mixture in a Venturi (Muir and Eichorn, 1963, 1967; Sandhu and Jameson, 1979). Wang and Brennen (1998) predict similar behaviour when a bubbly fluid passes through a Venturi. Note, however, that in the computation presented here the fixed exit pressure $p_{\text{exit}} = -2.09$, given by Eq. (35), is negative and hence unrealistic.

5.5. The effect of bubble radius R_0

We now change the bubble radius R_0 while holding the pressure constant. We present results in which $p_0^{\text{g}} = 200$ is held fixed, so that $M = p_0^{\text{g}} V_0$ varies as the bubble radius is changed. The effect of surface tension will vary when the bubble size is changed and one might argue that $p_0^{\text{g}} - 2\sigma/R_0$ should be held constant, rather than p_0^{g}. However, when $\sigma = 1.0$ changes in σ/R_0 are small compared to p_0^{g} and we neglect such effects.

Fig. 26 shows the differential pressure Δp generated by the passage of bubbles through a Venturi with $\beta = 0.5$. As might be expected, larger bubbles create greater changes to Δp. Motion of the bubble through such a narrow Venturi is rapid.

Estimates of the change in differential pressure Δp, due to the passage of the bubble, may be obtained using the one-dimensional model of Section 2.1. If the bubble is small compared to the throat radius we may take the added mass coefficient to be $C_{\text{m}} = \frac{1}{2}$. Assuming uniform flow (5) across the cross-section, the velocity of liquid at the centre of the throat is β^{-2} whereas by Eq. (4) the velocity of the bubble is $v_{\text{b}} = (3\beta^{-4} - 2)^{1/2}$. In the frame in which the

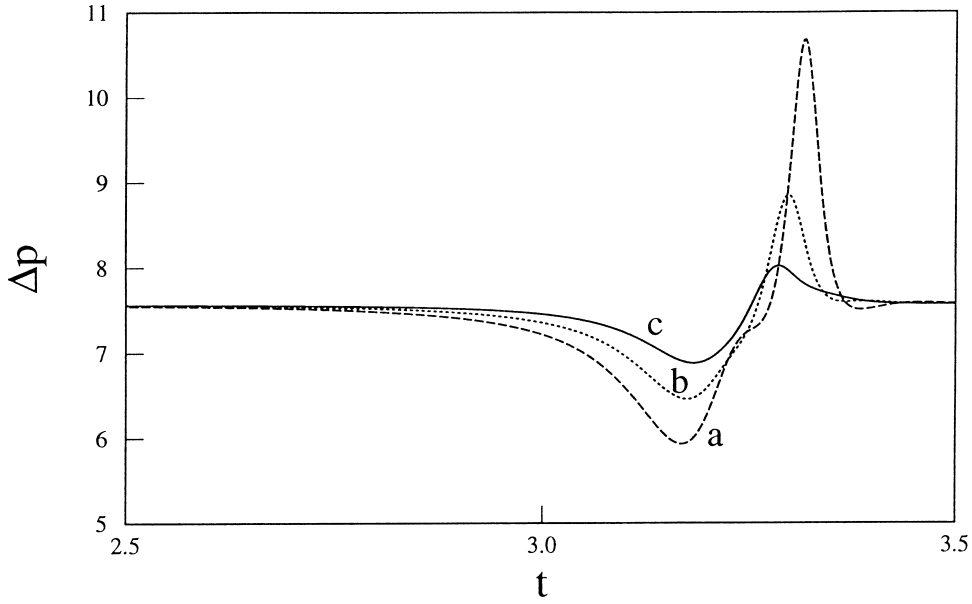

Fig. 26. Variation of differential pressure $\Delta p = p_1 - p_4$ as a function of bubble radius (a) $R_0 = 0.3$, (b) $R_0 = 0.25$, (c) $R_0 = 0.2$. $\beta = 0.5$, $p_0^{\text{g}} = 200$, $\sigma = 1.0$.

bubble is at rest, the liquid velocity within the throat is $v_0 = (3\beta^{-4} - 2)^{1/2} - \beta^{-2}$ far from the bubble. It can be shown from the potential flow analysis of Smythe (1961) that if the pipe is a uniform cylinder of radius β and the bubble is a sphere of radius $R_0 \ll \beta$, the velocity at the wall in this frame changes from v_0 far from the bubble to $v_0(1 + 1.776(R_0/\beta)^3 + \ldots)$ at points on the wall closest to the bubble. The wall pressure consequently decreases by $1.776 v_0^2 \rho_l (R_0/\beta)^3 + \ldots$. We therefore expect that when the bubble passes the centre of the Venturi, where the wall pressure p_4 is computed, the non-dimensional differential pressure Δp will increase to

$$\Delta p = \Delta p_l + 1.776\left[\left(3\beta^{-4} - 2\right)^{1/2} - \beta^{-2}\right]^2 \left(\frac{R_0}{\beta}\right)^3, \tag{40}$$

where the differential pressure Δp_l in the absence of any bubble is given by Eq. (12). If $R_0 = 0.1$ and $\beta = 0.5$, the numerical simulations indicate that Δp changes from $\Delta p_l = 7.566$ to a maximum 7.640 i.e. by 0.074, whereas Eq. (40) predicts a change 0.11.

If a force $F_a = -(4/3)\pi R_0^3 \rho_l D_l u_l / Dt$ is applied to the bubble the one-dimensional force balance, (2), predicts that the bubble moves with the liquid. If the bubble is small, the differential pressure across the Venturi will be unchanged from that for a homogeneous liquid (12). An applied force F_a leads to a difference between the pressures upstream and downstream of the bubble of magnitude $F_a/\pi R_p^2$ (Cai and Wallis, 1992; Sherwood and Stone, 1997), where R_p is the local radius of the pipe and where we have neglected any change in R_p over the small lengthscale R_0 of the bubble. Removing the force F_a will modify the non-dimensional differential pressure by an amount $(8/3)R_0^3 R_p^{-7} \mathrm{d}R_p/\mathrm{d}x$. This change in Δp is maximum when the bubble is just about to leave the converging section of the Venturi, when we expect the differential pressure to be

$$\Delta p = \Delta p_l - \frac{8R_0^3}{3\beta^7}\left(\frac{1-\beta}{x_2 - x_1}\right). \tag{41}$$

If $R_0 = 0.1$, $\beta = 0.5$ and $x_2 - x_1 = 1$ the numerical simulations predict that Δp is reduced by 0.122 to a minimum 7.444. The estimate (41) predicts a change 0.171. The potential flow velocity along the centreline varies more slowly than the approximation $u_l = R_p^{-2}$ (Fig. 7), so that Eq. (41) is based on an over-estimate of the extension rate just before the throat.

6. Concluding remarks

The computations predict that if the bubble oscillates on emerging from the Venturi, it also emerges more slowly than the surrounding liquid. Such translation is consistent with analyses by Saffman (1967), Miloh and Galper (1993) and Galper and Miloh (1995), but it is not clear why the bubble always emerges travelling more slowly than the liquid. In real life viscous drag would eventually reduce the relative velocity to zero. Weak viscous effects at a gas–liquid interface might be included in the manner discussed by Lundgren and Mansour (1988).

We have seen in Sections 5.1 and 5.2 that if the bubble is small and remains spherical the one-dimensional model of Section 2.1 can be used to predict its motion. This model is

sufficiently simple that it can be used to predict the motion of bubbles off the axis of the Venturi, and it can be extended to include drag: results will be reported elsewhere (Soubiran and Sherwood, 2000).

The differential pressure Δp between the entrance to the Venturi and the throat is modified, not only when the bubble accelerates through the converging section of the Venturi, but also when the pressure tapping in the throat detects liquid velocity fluctuations in the neighbourhood of the bubble. Modern rigorous derivations of two-fluid equations for dilute bubbly flows (e.g. Zhang and Prosperetti, 1994) include the effects of such fluctuations. The results obtained in Section 5 indicate that the fluctuations give rise to a significant contribution to time-averaged changes in Δp due to the passage of bubbles.

Acknowledgements

I thank J. Soubiran for results shown in Fig. 17, and Professor H. Stone both for suggesting the analysis of Appendix A and for helpful discussions supported by the NATO Collaborative Research Grant Programme (CRG.961165).

Appendix A. Frequency of bubble oscillation in a straight tube

A.1. Introduction

We consider small-amplitude oscillations of a gas-filled bubble such that the bubble remains spherical with radius R_0 a function of time t. A bubble surrounded by unbounded incompressible inviscid fluid was studied by Minnaert (1933), as discussed in the review by van Wijngaarden (1972). In unbounded fluid the fluid velocity $\boldsymbol{u}$ is radial with $u_r \propto r^{-2}$, where r is the distance from the bubble centre. The kinetic energy therefore decays as r^{-4} and is integrable. If the oscillating bubble is in a liquid-filled pipe, the liquid motion far from the bubble will be along the axis of the pipe, and in the absence of compressibility the liquid motion will not decay with distance from the bubble. The kinetic energy of the liquid therefore depends upon the length of the pipe, as does the frequency of oscillation of the bubble. The problem was recently studied by Oguz and Prosperetti (1998), but the analysis presented here is somewhat different and leads (after various approximations) to a closed expression for the oscillation frequency which is independent of the cross-section of the pipe. In addition we predict the slow drift of an oscillating bubble along the pipe axis. In Section A.5, the analytic predictions for the period of oscillation and rate of drift are compared against numerical simulations which use the boundary integral method described in Section 4. Agreement between analysis and simulation is good, even when the bubble radius is comparable with that of the tube. This forms a valuable check on the accuracy of the boundary integral computations of Section 5.

In the main body of the paper the liquid was assumed incompressible. We now relax this restriction, in part in order to show the conditions under which this assumption is reasonable, and in part in order to build upon previous work by Morse and Ingard (1968), who discuss the

Green's function for an oscillating point source in an infinitely long duct filled with compressible liquid. We consider here a finite duct and assume that the liquid compressibility is sufficiently small that the pipe is short compared to the wavelength of the sound waves. One end of the pipe is open and at constant pressure; at the other end we assume an arbitrary admittance, so that this second end may be considered either to be open, or to be closed by a rigid wall.

The liquid is at rest apart from oscillations generated by the bubble, so that $U = 0$ and the non-dimensionalisations of Sections 2–5 are therefore inappropriate. The analysis will be presented in dimensional form, and an alternative non-dimensionalisation will be adopted in Section A.5 when comparing numerical results with the analysis.

A.2. The Green's function of Morse and Ingard

The Green's function g_ω for a small amplitude (linear) sound wave generated by an oscillating source in an unbounded liquid-filled pipe is given by Morse and Ingard (1968, Section 9.2 of their work). Their analysis can be extended in a straightforward way to include pipes of finite length. We define a function Ψ such that the pressure p and liquid velocity $\boldsymbol{u}$ are

$$p = \rho_1 \frac{\partial \Psi}{\partial t}, \qquad \boldsymbol{u} = -\nabla \Psi. \tag{A1}$$

Ψ satisfies the wave equation

$$\frac{\partial^2 \Psi}{\partial t^2} = c^2 \nabla^2 \Psi, \tag{A2}$$

where c is the velocity of sound.

We consider a point source placed at (x_0, y_0, z_0) oscillating with time dependence $\exp(-i\omega t)$, for which Ψ may be written in the form $\Psi = g_\omega \exp(-i\omega t)$, where g_ω satisfies

$$\left[\frac{\partial^2}{\partial x^2} + \frac{\partial^2}{\partial y^2} + \frac{\partial^2}{\partial z^2} + \left(\frac{\omega}{c}\right)^2\right] g_\omega(x, y, x|x_0, y_0, z_0) = -\delta(x - x_0)\delta(y - y_0)\delta(z - z_0). \tag{A3}$$

The boundary conditions that g_ω must satisfy take the form

$$\boldsymbol{u} \cdot \boldsymbol{n} = \frac{\beta_a p}{\rho_1 c} \tag{A4}$$

where $\boldsymbol{n}$ is the outwards facing normal and β_a is the admittance, with $\beta_a = 0$ if the boundary is a rigid wall and $\beta_a^{-1} = 0$ if the pressure is constant on the boundary. Thus,

$$\frac{\partial g_\omega}{\partial n} = ik\beta_a g_\omega, \quad k = \frac{\omega}{c}. \tag{A5}$$

Morse and Ingard considered a source within an infinite pipe, and required that g_ω decayed as $|x| \to \infty$. We shall instead consider a finite pipe occupying the region $x_1 \leq x \leq x_2$ (Fig. A1). The admittance will be β_1 at $x = x_1$. We assume that the admittance at $x = x_2$ is infinite, so that

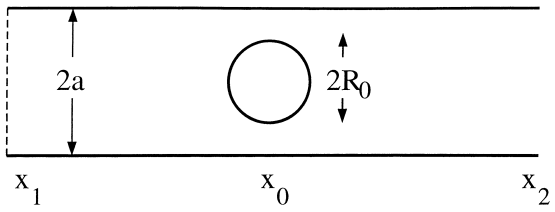

Fig. A1. The bubble of radius R_0 in a pipe of radius a.

the pressure there is constant and fluctuations in pressure are zero. The pipe walls are assumed to be rigid.

We follow Morse and Ingard and look for an expansion of g_ω of the form

$$g_\omega = \sum_n F_n(x)\Psi_n(y, z) \tag{A6}$$

where the eigenfunctions $\Psi_n(y, z)$ satisfy

$$\left(\frac{\partial^2}{\partial y^2} + \frac{\partial^2}{\partial z^2}\right)\Psi_n = -\kappa_n^2\Psi_n \tag{A7}$$

together with the boundary condition (A5) on the pipe walls. The eigenvalues κ_n depend upon the detailed cross-sectional geometry. The Ψ_n are chosen so as to be mutually orthogonal, with

$$\int_S \Psi_n\Psi_m \,\mathrm{d}S = \delta_{nm}S\Lambda_n, \tag{A8}$$

where S is the cross-sectional area of the pipe.

Inserting Eq. (A6) into the differential equation (A3), multiplying by Ψ_n and integrating over S leads to

$$\left(\frac{\mathrm{d}^2}{\mathrm{d}x^2} + k_n^2\right)F_n = -\frac{\Psi_n(y_0, z_0)}{S\Lambda_n}\delta(x - x_0) \tag{A9}$$

where

$$k_n^2 = \left(\frac{\omega}{c}\right)^2 - \kappa_n^2. \tag{A10}$$

When the walls are rigid the eigenfunctions Ψ_n are real, and the eigenvalues κ_n are real and non-negative, with $\Psi_0 = 1$ and $\kappa_0 = 0$. For definiteness, when $\omega/c > \kappa_n$ we set

$$k_n = \left[\left(\frac{\omega}{c}\right)^2 - \kappa_n^2\right]^{1/2}. \tag{A11}$$

There will be some value of $n = N$ such that $\kappa_n > \omega/c$ for $n > N$, and we set

$$K_n = \left[\kappa_n^2 - \left(\frac{\omega}{c}\right)^2\right]^{1/2}, \quad n > N. \tag{A12}$$

At this point in their analysis of an infinite pipe, Morse and Ingard require that the F_n decay as $|x|\to\infty$, and look for solutions of the form $F_n \propto \exp(ik_n|x - x_0|)$. In our finite pipe, we instead require

$$F_n = 0, \qquad x = x_2 \tag{A13a}$$

$$ik\beta_1 F_n = -\frac{\mathrm{d}F_n}{\mathrm{d}x}, \quad x = x_1 \tag{A13b}$$

and hence we look for a function F_n of the form

$$F_n = A_n\left[\left(\frac{k_n}{k} - \beta_1\right)\mathrm{e}^{ik_n(x-x_1)} + \left(\frac{k_n}{k} + \beta_1\right)\mathrm{e}^{-ik_n(x-x_1)}\right], \quad x_1 \le x \le x_0 \tag{A14a}$$

$$F_n = B_n\left[\mathrm{e}^{ik_n(x-x_2)} - \mathrm{e}^{-ik_n(x-x_2)}\right], \qquad x_0 < x < x_2. \tag{A14b}$$

Continuity at $x = x_0$ requires

$$A_n\left[\left(\frac{k_n}{k} - \beta_1\right)\mathrm{e}^{ik_n(x_0-x_1)} + \left(\frac{k_n}{k} + \beta_1\right)\mathrm{e}^{-ik_n(x_0-x_1)}\right] = B_n\left[\mathrm{e}^{ik_n(x_0-x_2)} - \mathrm{e}^{-ik_n(x_0-x_2)}\right]. \tag{A15}$$

By Eq. (A9) there is a jump condition

$$\left[F_n'\right]_{x_0^-}^{x_0^+} = -\frac{\Psi_n(y_0, z_0)}{S\Lambda_n}. \tag{A16}$$

Hence

$$A_n = -\left(\frac{k\Psi_n(y_0, z_0)}{2ik_n S\Lambda_n}\right)\frac{\mathrm{e}^{ik_n(x_0-x_2)} - \mathrm{e}^{-ik_n(x_0-x_2)}}{(k_n - k\beta_1)\mathrm{e}^{ik_n(x_2-x_1)} + (k_n + k\beta_1)\mathrm{e}^{-ik_n(x_2-x_1)}} \tag{A17a}$$

and

$$B_n = -\left(\frac{\Psi_n(y_0, z_0)}{2ik_n S\Lambda_n}\right)\frac{(k_n - k\beta_1)\mathrm{e}^{ik_n(x_0-x_1)} + (k_n + k\beta_1)\mathrm{e}^{-ik_n(x_0-x_1)}}{(k_n - k\beta_1)\mathrm{e}^{ik_n(x_2-x_1)} + (k_n + k\beta_1)\mathrm{e}^{-ik_n(x_2-x_1)}}. \tag{A17b}$$

In $x > x_0$

$$g_\omega = \frac{i}{S}\sum_n \frac{\Psi_n(y_0,z_0)\Psi_n(y,z)}{k_n\Lambda_n}\frac{\left[k_n\cos k_n(x_0-x_1)-ik\beta_1\sin k_n(x_0-x_1)\right]i\sin k_n(x-x_2)}{k_n\cos k_n(x_2-x_1)-ik\beta_1\sin k_n(x_2-x_1)}$$

$$= -\frac{1}{kS}\frac{\left[\cos k(x_0-x_1)-i\beta_1\sin k(x_0-x_1)\right]\sin k(x-x_2)}{\cos k(x_2-x_1)-i\beta_1\sin k(x_2-x_1)}$$

$$-\frac{1}{S}\sum_{n=1}^{N}\frac{\Psi_n(y_0,z_0)\Psi_n(y,z)}{k_n\Lambda_n}\frac{\left[k_n\cos k_n(x_0-x_1)-ik\beta_1\sin k_n(x_0-x_1)\right]\sin k_n(x-x_2)}{k_n\cos k_n(x_2-x_1)-ik\beta_1\sin k_n(x_2-x_1)}$$

$$-\frac{1}{S}\sum_{n=N+1}^{\infty}\frac{\Psi_n(y_0,z_0)\Psi_n(y,z)}{K_n\Lambda_n}\frac{\left[K_n\cosh K_n(x_0-x_1)-k\beta_1\sinh K_n(x_0-x_1)\right]\sinh K_n(x-x_2)}{K_n\cosh K_n(x_2-x_1)-k\beta_1\sinh K_n(x_2-x_1)} \tag{A18}$$

We now expand the radial distance $R=[(x-x_0)^2+(y-y_0)^2+(z-z_0)^2]^{1/2}$ from the source in terms of the eigenfunctions Ψ_n, using the expression (Morse and Ingard, 1968, p. 501)

$$\lim_{R\to 0}\left\{\frac{1}{4\pi R}\right\} = -\frac{|x-x_0|}{2S}+\frac{1}{2S}\sum_{n=1}^{\infty}\frac{\Psi_n(y,z)\Psi_n(y_0,z_0)}{\Lambda_n\kappa_n}\exp(-\kappa_n|x-x_0|) \tag{A19}$$

and we assume that the pipe is sufficiently long (compared to K_{N+1}^{-1}) and the bubble sufficiently far from the ends of the pipe, that

$$\frac{\sinh K_n(x_0-x_1)\sinh K_n(x-x_2)}{\sinh K_n(x_2-x_1)} \approx -\tfrac{1}{2}\exp\left[K_n(x_0-x)\right] \quad \text{for} \quad x>x_0,\ n\geq N. \tag{A20}$$

Combining Eqs. (A18) and (A19), we have

$$g_\omega \simeq \frac{1}{4\pi R}+\frac{|x-x_0|}{2S}-\frac{1}{kS}\frac{\left[\cos k(x_0-x_1)-i\beta_1\sin k(x_0-x_1)\right]\sin k(x-x_2)}{\cos k(x_2-x_1)-i\beta_1\sin k(x_2-x_1)}$$

$$-\frac{1}{S}\sum_{n=1}^{N}\frac{\Psi_n(y_0,z_0)\Psi_n(y,z)}{\Lambda_n}\left(\frac{\left[k_n\cos k_n(x_0-x_1)-ik\beta_1\sin k_n(x_0-x_1)\right]\sin k_n(x-x_2)}{k_n\left[k_n\cos k_n(x_2-x_1)-ik\beta_1\sin k_n(x_2-x_1)\right]}\right.$$

$$\left.+\frac{\exp(-\kappa_n|x-x_0|)}{2\kappa_n}\right). \tag{A21}$$

Cases in which the denominators of the various terms in Eq. (A21) become zero correspond to resonances of the entire column of compressible liquid. Thus, if $\beta_1=0$ a first resonance occurs when $x_2-x_1=\pi/2k$, whereas in the limit $\beta_1\to\infty$ we require $x_2-x_1=\pi/k$.

We now let the compressibility of the liquid tend to zero so that such resonances are avoided. As $c\to\infty$, so $k\to 0$ and $\kappa_n>\omega/c$ for all $n\geq 1$, and hence $N=0$. In this case, in the limit $R\to 0$, g_ω takes the simple form

$$g_\omega \simeq \frac{1}{4\pi R} + \frac{x - x_0}{2S} - \frac{(x - x_2)}{S}\left(\frac{1 - i\beta_1 k(x_0 - x_1)}{1 - i\beta_1 k(x_2 - x_1)}\right) \quad R \to 0,\ x > x_0. \tag{A22a}$$

independent of the detailed pipe shape; a similar analysis in $x < x_0$ leads to

$$g_\omega \simeq \frac{1}{4\pi R} + \frac{x_0 - x}{2S} - \frac{(x_0 - x_2)}{S}\left(\frac{1 - i\beta_1 k(x - x_1)}{1 - i\beta_1 k(x_2 - x_1)}\right) \quad R \to 0,\ x < x_0. \tag{A22b}$$

Sufficiently close to the source $R^2 \ll S$, so that the dominant contribution to the liquid velocity $\boldsymbol{u} = -\nabla\Psi$ is radial, with

$$u_r \sim \frac{\mathrm{e}^{-i\omega t}}{4\pi R^2} \quad R^2 \ll S. \tag{A23}$$

The pressure in the limit $R \to 0$ (and thus in the limit $x \to x_0$) can be obtained from either Eq. (A22a) or Eq. (A22b) and is

$$p = -i\omega\rho_1 \mathrm{e}^{-i\omega t}\left[\frac{1}{4\pi R} - \frac{(x_0 - x_2)}{S}\left(\frac{1 - i\beta_1 k(x_0 - x_1)}{1 - i\beta_1 k(x_2 - x_1)}\right)\right]. \tag{A24}$$

If $x - x_0 \gg \kappa_1^{-1}$, then by Eq. (A18) in the limit $k \to 0$, $N = 0$

$$g_\omega \simeq -\frac{(x - x_2)}{S}\left(\frac{1 - i\beta_1 k(x_0 - x_1)}{1 - i\beta_1 k(x_2 - x_1)}\right) \quad x - x_0 \gg \kappa_1^{-1} \tag{A25a}$$

and similarly in $x < 0$

$$g_\omega \simeq -\frac{(x_0 - x_2)}{S}\left(\frac{1 - i\beta_1 k(x - x_1)}{1 - i\beta_1 k(x_2 - x_1)}\right) \quad x_0 - x \gg \kappa_1^{-1}, \tag{A25b}$$

so that the liquid velocity is uniform across the pipe cross-section far from the bubble.

A.3. The source strength of an oscillating bubble

We now have expressions for the pressure and velocity fields due to a point source, and must determine the source strength of an oscillating bubble. We suppose that at equilibrium the bubble contains gas at pressure p_0^{g} and that the bubble radius R_0 is small compared to the distance of the bubble from the walls of the pipe. The interfacial tension between gas and liquid is σ. The oscillations of the bubble are assumed to be adiabatic, so that $p^{\mathrm{g}}V^{\gamma}$is constant, where p^{g} is the gas pressure, V the gas volume and γ the ratio of the specific heats of the gas. If we take $\gamma = 1$ we recover the isothermal ideal gas law. The pressure at the open end (or ends) of the pipe is assumed to be constant, and equal to $p_0^{\mathrm{g}} - 2\sigma/R_0$, so that pressure perturbations at the end of the pipe are zero. If the radius of the bubble changes from R_0 to

$$R_{\mathrm{b}} = R_0\left(1 + \delta \mathrm{e}^{-i\omega t}\right) \tag{A26}$$

the pressure within the gas bubble is

$$p^{\mathrm{g}} = p_0^{\mathrm{g}}\left(1 - 3\gamma\delta \mathrm{e}^{-i\omega t}\right) \tag{A27}$$

and the pressure in the liquid adjacent to the bubble is

$$p = p_0^{\mathrm{g}} - \frac{2\sigma}{R_0} - \delta \mathrm{e}^{-i\omega t}\left(3\gamma p_0 - \frac{2\sigma}{R_0}\right). \tag{A28}$$

The velocity at the surface of the bubble is

$$u_r = -i\omega R_0 \delta \mathrm{e}^{-i\omega t}. \tag{A29}$$

If we compare this with Eq. (A23) we see that the bubble is behaving as a source of strength

$$S_\omega = -4\pi i\omega R_0^3 \delta. \tag{A30}$$

Equating the oscillatory component of pressure immediately outside the bubble (A28) to the pressure (A24) generated by a point source, we obtain

$$\omega^2 = \frac{\left(3\gamma p_0^{\mathrm{g}} - 2\sigma R_0^{-1}\right)}{R_0^2 \rho_1}\left[1 - \frac{4\pi R_0 (x_0 - x_2)}{S}\left(\frac{1 - i\beta_1 k(x_0 - x_1)}{1 - i\beta_1 k(x_2 - x_1)}\right)\right]^{-1}. \tag{A31}$$

In general, energy is lost at a non-rigid barrier at x_1, and the frequency, (A31) is complex, corresponding to an oscillation that decays. If the pipe is open at x_1, with β_1 infinite, then

$$\omega^2 = \frac{\left(3\gamma p_0^{\mathrm{g}} - 2\sigma R_0^{-1}\right)}{R_0^2 \rho_1}\left[1 + \frac{4\pi R_0 (x_2 - x_0)}{S}\left(\frac{x_0 - x_1}{x_2 - x_1}\right)\right]^{-1}. \tag{A32}$$

If the pipe is closed by a rigid barrier, then $\beta_1 = 0$ and

$$\omega^2 = \frac{\left(3\gamma p_0^{\mathrm{g}} - 2\sigma R_0^{-1}\right)}{R_0^2 \rho_1}\left[1 + \frac{4\pi R_0 (x_2 - x_0)}{S}\right]^{-1}, \tag{A33}$$

which corresponds to Eq. (A32) in the limit $x_1 \to -\infty$. We see that the effect of the pipe is to increase the inertia of the oscillating liquid, and thereby decrease the frequency of oscillation of the bubble. It is perhaps worth re-stating that the analysis has assumed that the various length scales R_0 (bubble radius), a (typical length-scale for the pipe cross-section), L (pipe length) and $2\pi/k$ (wavelength of sound) satisfy $R_0 \ll a \ll L \ll 2\pi/k$.

Oguz and Prosperetti (1998) compared their results against a one-dimensional slug model. If a gas slug with initial volume V_0 and pressure p_0^{g} causes a single slug of liquid of length $x_2 - x_0$ to oscillate, an analysis similar to that in Section 2.2 predicts that frequency of oscillation ω satisfies

$$\omega^2 = \frac{p_0^{\mathrm{g}} \gamma S}{V_0 \rho_1 (x_2 - x_0)}. \tag{A34}$$

This corresponds to Eq. (A33) in the limit $x_2 - x_0 \gg R_0$ when surface tension is negligible. If two slugs of lengths $x_0 - x_1$ and $x_2 - x_0$ oscillate, then

$$\omega^2 = \frac{p_0^{\mathrm{g}} \gamma S(x_2 - x_1)}{V_0 \rho_1 (x_2 - x_0)(x_0 - x_1)} \tag{A35}$$

which corresponds to Eq. (A32). The inertia of the system is dominated by that of the long columns of liquid moving parallel to the axis of the pipe, rather than by the liquid which moves radially in the vicinity of the bubble.

A.4. Drift

The liquid motion in the neighbourhood of the bubble can be obtained by taking the gradient of either Eq. (A22a) or Eq. (A22b), and consists of a radial flow, together with a background axial drift of the liquid

$$U_{\mathrm{d}}(x_0) = \frac{S_\omega \mathrm{e}^{-i\omega t}}{2S}, \qquad \beta_1 = 0 \tag{A36a}$$

$$U_{\mathrm{d}}(x_0) = -\left(\frac{x_2 + x_1 - 2x_0}{x_2 - x_1}\right)\frac{S_\omega \mathrm{e}^{-i\omega t}}{2S}, \quad \beta_1 = \infty \tag{A36b}$$

where the source strength S_ω is given by Eq. (A30). From Eq. (A36b) we see that if the configuration is symmetric, the background drift $U_{\mathrm{d}} = 0$, as expected. The pressure gradient in the neighbourhood of the bubble similarly consists of the pressure gradient associated with radial flow around the bubble (which we shall ignore), together with a background gradient.

$$\frac{\partial p_{\mathrm{d}}}{\partial x} = -\frac{\partial U_{\mathrm{d}}}{\partial t}. \tag{A37}$$

The bubble has zero mass, and we assume that it translates with a velocity v_{b} which in general will differ from the velocity of the liquid. We assume that the bubble is sufficiently small that the acceleration reaction (added mass force) acting on the bubble is as in unbounded liquid: this assumption is reasonable since the far field due to translation of the bubble is a dipole, which decays more rapidly than the monopole due to the oscillation of the bubble volume. In the absence of gravity the force balance on the bubble is given by Batchelor (1973, p. 455):

$$0 = \frac{4\pi R_{\mathrm{b}}^3}{3}\frac{\mathrm{d}U_{\mathrm{d}}}{\mathrm{d}t} + \frac{1}{2}\frac{\mathrm{d}}{\mathrm{d}t}\left[\frac{4\pi R_{\mathrm{b}}^3}{3}(U_{\mathrm{d}} - v_{\mathrm{b}})\right] \tag{A38}$$

so that

$$\frac{\mathrm{d}v_{\mathrm{b}}}{\mathrm{d}t} = 3\frac{\mathrm{d}U_{\mathrm{d}}}{\mathrm{d}t} - (v_{\mathrm{b}} - U_{\mathrm{d}})\frac{3}{R_{\mathrm{b}}}\frac{\mathrm{d}R_{\mathrm{b}}}{\mathrm{d}t}. \tag{A39}$$

The fluctuating part of v_{b} is approximately $3U_{\mathrm{d}}$, and the average acceleration of the bubble over a cycle is

$$\overline{\frac{\mathrm{d}v_\mathrm{b}}{\mathrm{d}t}} = -\frac{6\pi\omega^2 R_0^3\delta^2}{S}, \quad \beta_1 = 0 \tag{A40a}$$

$$= \left(\frac{x_2 + x_1 - 2x_0}{x_2 - x_1}\right)\frac{6\pi\omega^2 R_0^3\delta^2}{S}, \quad \beta_1 = \infty. \tag{A40b}$$

If one end of the pipe is closed, the bubble will accelerate towards this end, as might be expected from the classical analysis for two bubbles in unbounded liquid, equivalent to that for one bubble in the presence of an infinite plane wall. If both ends of the pipe are open, the bubble will drift towards the centre of the pipe. The attraction between bubbles oscillating in phase, or repulsion when out of phase, was known to C.A. Bjerknes, and details are given by Bjerknes (1900). Other references are cited by Lamb (1932, p. 134).

Note that to obtain Eqs. (A40a) and (A40b) we have neglected terms which, though small, depend upon the position (y_0, z_0) of the bubble within a cross-sectional plane. Slow drift perpendicular to the axis of the pipe is therefore neglected. Since the radius of the pipe is small compared to its length, this radial drift may ultimately be important.

A.5. Comparison with numerical work

We now use these results to check the accuracy of the numerical code described in Section 4. Computations were performed with the inlet velocity $U = 0$ and Venturi throat diameter $\beta = 1$, so that the pipe was straight with zero flow at the entrance, corresponding to an admittance $\beta_1 = 0$.

We scale lengths by the pipe radius a, pressures by M/a^3, velocities by $(M/\rho_1 a^3)^{1/2}$, and time by $(\rho_1 a^5/M)^{1/2}$. Non-dimensional quantities are denoted by a circumflex ($\hat{}$). The non-dimensional interfacial tension $\hat{\sigma} = \sigma a^2/M = 0.01$ so that the effect of interfacial tension was negligible. The initial volume of the bubble differed from that of a bubble at equilibrium by 1%, so that $\delta = 0.00333$ in Eq. (A26).

The period of oscillation is predicted by Eq. (A33) to be

$$\hat{T} = \frac{2\pi}{\hat{\omega}} = \frac{2\pi\hat{R}_0}{\left(3\hat{p}_0^\mathrm{g}\right)^{1/2}}\left[1 + 4\hat{R}_0(\hat{x}_2 - \hat{x}_0)\right]^{1/2} = \frac{4\pi\hat{R}_0^2}{3}\left(\pi\hat{R}_0\right)^{1/2}\left[1 + 4\hat{R}_0(\hat{x}_2 - \hat{x}_0)\right]^{1/2}, \tag{A41}$$

and the non-dimensional acceleration towards the rigid end of the pipe is (A40a):

$$\overline{\frac{d\hat{v}_\mathrm{b}}{d\hat{t}}} = -6\hat{\omega}^2\hat{R}_0^3\delta^2. \tag{A42}$$

In Figs. A2–A4, the analytic predictions (A41) are shown as curves, and simulation results are shown as individual points. In Fig. A2, we see results for the period of oscillation $\hat{T}$ as a function of bubble radius $\hat{R}_0$ in a pipe with $\hat{x}_0 - \hat{x}_1 = 6$, $\hat{x}_2 - \hat{x}_0 = 5$. Agreement is good for small bubbles, and also for bubbles which are only slightly smaller than the pipe diameter. As discussed in Section A.3, if the pipe is sufficiently long the fine details of the flow in the region $|x - x_0| \simeq a$ are no longer important in determining the frequency of oscillation, and we see

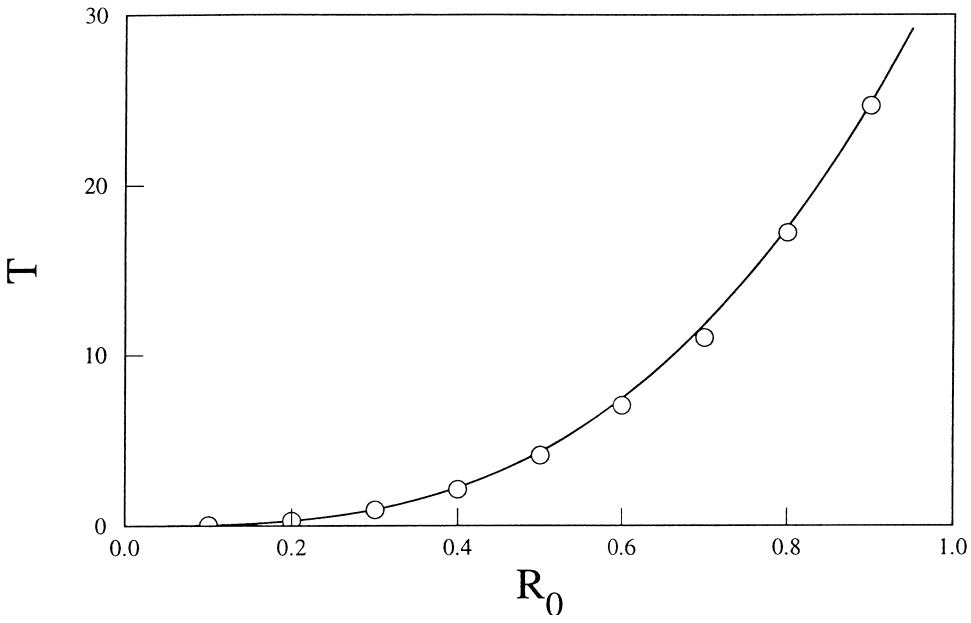

Fig. A2. The non-dimensional period $\hat{T}$ as a function of bubble radius $\hat{R}_0$. $\hat{x}_2 - \hat{x}_0 = 5$, $\hat{x}_0 - \hat{x}_1 = 6$. Analytic prediction (A41) ——— ; numerical simulation ○.

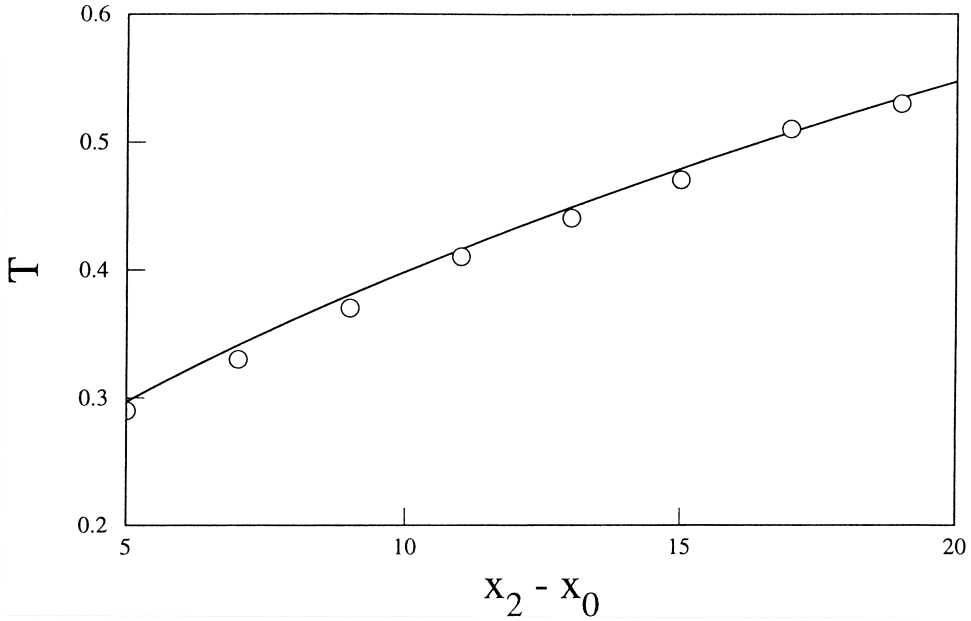

Fig. A3. The non-dimensional period $\hat{T}$ as a function of $\hat{x}_2 - \hat{x}_0$. Bubble radius $\hat{R}_0 = 0.2$, $\hat{x}_0 - \hat{x}_1 = 6$. Analytic prediction (A41) ———; numerical simulation ○.

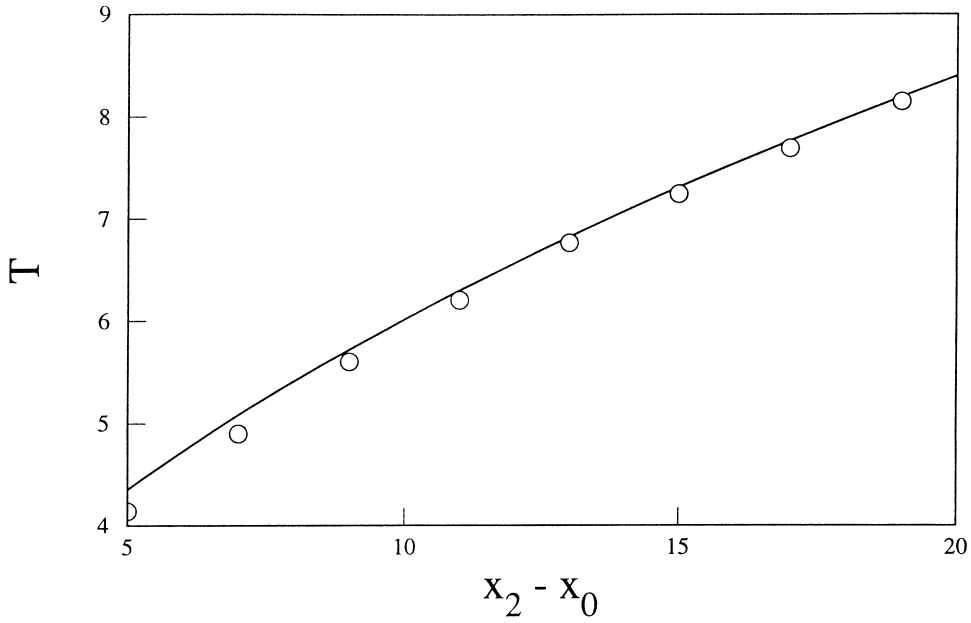

Fig. A4. The non-dimensional period $\hat{T}$ as a function of $\hat{x}_2 - \hat{x}_0$. Bubble radius $\hat{R}_0 = 0.5$, $\hat{x}_0 - \hat{x}_1 = 6$. Analytic prediction (A41) ———; numerical simulation ○.

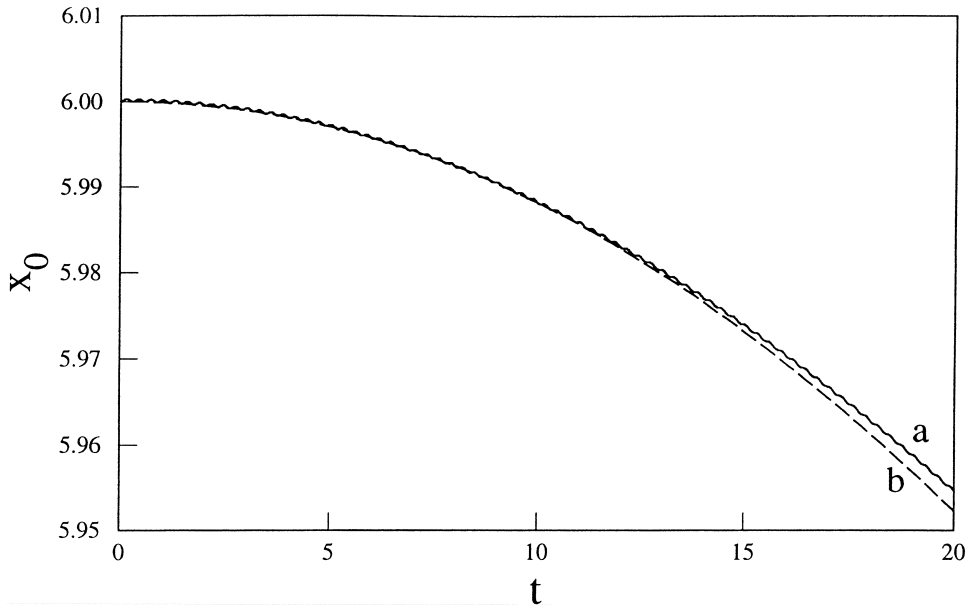

Fig. A5. The position $\hat{x}_0$ of an oscillating bubble of radius $\hat{R}_0 = 0.2$ as it drifts in a tube closed at $\hat{x}_1 = 0$ and open at $\hat{x}_2 = 11$. (a) Numerical simulation ———; (b) analytic prediction (A42) – – – .

from Eq. (A41) that this is the case when $4\hat{R}_0(\hat{x}_2 - \hat{x}_0) \gg 1$. The effect of pipe length is shown in Fig. A3 for bubbles of radius $\hat{R}_0 = 0.2$ and in Fig. A4 for $\hat{R}_0 = 0.5$. In both cases $\hat{x}_0 - \hat{x}_1 = 6$ is fixed and $\hat{x}_2 - \hat{x}_0$ is allowed to vary. Agreement is excellent, especially when the pipe becomes long.

In Fig. A5 we see the position $\hat{x}_0$ of the centre of a bubble which oscillates in a tube closed at $\hat{x}_1 = 0$ and open at $\hat{x}_2 = 11$. The bubble accelerates towards the closed end, as predicted by Eq. (A42). Differences between the numerical simulation and the analysis of Section A.4 are only noticeable at long times. Since the bubble is on the axis of symmetry, we do not expect any drift in the radial direction.

References

Abramowitz, M., Stegun, I.A., 1964. Handbook of Mathematical Tables. Dover, New York.

Auton, T.T., Hunt, J.C.R., Prudhomme, M., 1988. The force exerted on a body in inviscid unsteady non-uniform rotational flow. J. Fluid Mech 197, 241–257.

Batchelor, G.K., 1973. An Introduction to Fluid Dynamics. Cambridge University Press, Cambridge.

Benjamin, T.B., 1989. Note on shape oscillations of bubbles. J. Fluid Mech 203, 419–424.

Best, J.P., Kucera, A., 1992. A numerical investigation of non-spherical rebounding bubbles. J. Fluid Mech 245, 137–154.

Bjerknes, V., 1900. Vorlesungen über hydrodynamische Fernkräfte, (2 vols.). Leipzig.

Boulton-Stone, J.M., Blake, J.R., 1993. Gas bubbles bursting at a free surface. J. Fluid Mech 254, 437–466.

Boulton-Stone, J.M., Robinson, P.B., Blake, J.R., 1995. A note on the axisymmetric interaction of pairs of rising, deformable gas bubbles. Int. J. Multiphase Flow 21, 1237–1241.

Boyer, C., Lemonnier, H., 1996. Design of a flow metering process for two-phase dispersed flows. Int. J. Multiphase Flow 22, 713–732.

British Standards Institution, 1997. BS EN ISO 5167-1. Measurement of fluid flow by means of pressure differential devices. British Standards Institution, London.

Cai, X., Wallis, G.B., 1992. Potential flow around a row of spheres in a circular tube. Phys. Fluids A 4, 904–912.

Dold, J.W., 1992. An efficient surface-integral algorithm applied to unsteady gravity waves. J. Comp. Phys 103, 90–115.

Duineveld, P.C., 1995. The rise velocity and shape of bubbles in pure water at high Reynolds number. J. Fluid Mech 292, 325–332.

Galper, A., Miloh, T., 1995. Dynamic equations of motion for a rigid or deformable body in an arbitrary non-uniform potential flow field. J. Fluid Mech 295, 91–120.

Jaswon, M.A., Symm, G.T., 1977. Integral Equation Methods in Potential Theory and Elastostatics. Academic Press, New York.

Kowe, R., Hunt, J.C.R., Hunt, A., Couet, B., Bradbury, L.J.S., 1988. The effects of bubbles on the volume fluxes and the pressure gradients in unsteady and non-uniform flow of liquids. Int. J. Multiphase Flow 14, 587–606.

Kuo, J.T., Wallis, G.B., 1988. Flow of bubbles through nozzles. Int. J. Multiphase Flow 14, 547–564.

Lamb, H., 1932. Hydrodynamics, 6th ed. Cambridge University Press, Cambridge.

Leighton, T.G., 1994. The Acoustic Bubble. Academic Press, New York.

Leyrat-Maurin, A., Barthès-Biesel, D., 1994. Motion of a deformable capsule through a hyperbolic constriction. J. Fluid Mech 279, 135–163.

Longuet-Higgins, M.S., 1989a. Monopole emission of sound by asymmetric bubble oscillations. Part 1. Normal modes. J. Fluid Mech 201, 525–541.

Longuet-Higgins, M.S., 1989b. Monopole emission of sound by asymmetric bubble oscillations. Part 2. An initial-value problem. J. Fluid Mech 201, 543–565.

Longuet-Higgins, M.S., 1989c. Some integral theorems relating to the oscillations of bubbles. J. Fluid Mech 204, 159–166.

Longuet-Higgins, M.S., 1991. Resonance in nonlinear bubble oscillations. J. Fluid Mech 224, 531–549.
Longuet-Higgins, M.S., Cokelet, E.D., 1976. The deformation of steep surface waves on water. I. Numerical methods of computation. Proc. R. Soc. London A 350, 1–26.
Lundgren, T.S., Mansour, N.N., 1988. Oscillations of drops in zero gravity with weak viscous effects. J. Fluid Mech 194, 479–510.
Lundgren, T.S., Mansour, N.N., 1991. Vortex ring bubbles. J. Fluid Mech 224, 177–196.
Miloh, T., Galper, A., 1993. Self-propulsion of general deformable shapes in a perfect fluid. Proc. R. Soc. London A 442, 273–299.
Minnaert, M., 1933. On musical air bubbles and sounds of running water. Phil. Mag 16, 235–248.
Moore, D.W., 1959. The rise of a gas bubble in a viscous liquid. J. Fluid Mech 6, 113–120.
Morse, P.M., Ingard, K.U., 1968. Theoretical Acoustics. McGraw-Hill, New York.
Muir, J.F., Eichorn, R., 1963. Compressible flow of an air–water mixture through a vertical, two-dimensional, converging–diverging nozzle. In: Proceedings of the 1963 Heat transfer and Fluid Mechanics Inst. Stanford University Press, Stanford.
Muir, J.F., Eichorn, R., 1967. Further studies of the compressible flow of an air–water mixture through a vertical, two-dimensional, converging diverging nozzle. In: JSME 1967 Semi-International Symposium, 4–8 Sept. 1967, vol. 2, Tokyo, 81–92.
Oguz, H.N., Prosperetti, A., 1989. Surface-tension effects in the contact of liquid surfaces. J. Fluid Mech 203, 149–171.
Oguz, H.N., Prosperetti, A., 1993. Bubble growth and detachment from a needle. J. Fluid Mech 257, 111–145.
Oguz, H.N., Prosperetti, A., 1998. The natural frequency of oscillation of gas bubbles in tubes. J. Acoustic. Soc. Am 103, 3301–3308.
Oldenziel, D.M., 1982. A new instrument in cavitation research: the cavitation susceptibility meter. J. Fluids Engineering 104, 136–142.
Press, W.H., Teukolsky, S.A., Vetterling, W.T., Flannery, B.P., 1992. Numerical Recipes in Fortran: The Art of Scientific Computing, 2nd ed. Cambridge University Press, Cambridge.
Saffman, P.G., 1967. The self-propulsion of a deformable body in a perfect fluid. J. Fluid Mech 28, 385–389.
Sandhu, N., Jameson, G.J., 1979. An experimental study of choked foam flows in a convergent–divergent nozzle. Int. J. Multiphase Flow 5, 39–58.
Sherwood, J.D., Stone, H.A., 1997. Added mass of a disc accelerating within a pipe. Phys. Fluids 9, 3141–3148.
Smythe, W.R., 1961. Flow around a sphere in a circular tube. Phys. Fluids 4, 756–759.
Soubiran, J., Sherwood, J.D., 2000. Bubble motion in a potential flow within a Venturi. Int. J. Multiphase Flow 26, 1771–1796.
Thorn, R., Johansen, G.A., Hammer, E.A., 1997. Recent developments in three-phase flow measurement. Meas. Sci. Technol 8, 691–701.
Tsai, T.M., Miksis, M.J., 1994. Dynamics of a drop in a constricted capillary tube. J. Fluid Mech 274, 197–217.
Udaykumar, H.S., Kan, H.-C., Shyy, W., Tran-Son-Tay, R., 1997. Multiphase dynamics in arbitrary geometries on fixed Cartesian grids. J. Comput. Phys 137, 366–405.
van Wijngaarden, L., 1972. One-dimensional flow of liquids containing small gas bubbles. Ann. Rev. Fluid Mech 4, 369–396.
Wang, Y.-C., Brennen, C.E., 1998. One-dimensional bubbly cavitating flows through a converging–diverging nozzle. J. Fluids Engng 120, 166–170.
Zhang, D.Z., Prosperetti, A., 1994. Ensemble phase-averaged equations for bubbly flows. Phys. Fluids 6, 2956–2970.